Interreg
EUROPEAN UNION
2 Seas Mers Zeeën
Polder2C's
European Regional Development Fund

Insights from Steady overflow and Wave overtopping tests

Adaptation to climate change

Interreg
2 Seas Mers Zeeën
Polder2C's
European Regional Development Fund

Insights from Steady overflow and Wave overtopping tests

Version:
20240612

Authors:
Depreiter, D.; Vercruysse, J.; Verelst, K.; Peeters, P.

Ref.:
WL2024R20_047_4_P2C_Overflow-Overtopping_Insights

This project has received funding from the Interreg 2 Seas programme 2014-2020 co-funded by the European Regional Development Fund under subsidy contract No [2S07-023]

Cover figure © INTERREG Polder2C's

Legal notice

Copyright and citation

This publication should be cited as follows:

Depreiter, D.; Vercruysse, J.; Verelst, K.; Peeters, P. (2023). Insights from Steady overflow and Wave overtopping tests. Version 4.0. FH Reports, 20_047_4. Flanders Hydraulics: Antwerp

Document identification

Customer:	Flanders Hydraulics	Ref.:	WL2023R20_047_4
Keywords (3-5):	Levee; Overflow, Overtopping, Field measurements		
Knowledge domains:	Hydraulic structures > Dikes, shores and other flood defenses > erosion protection > in-situ measurements		
Text (p.):	65	Appendices (p.):	/
Confidential:	☒ No	☒ Available online	

Author(s):	Depreiter, D.

Control

	Name	Signature
Reviser(s):	Vercruysse, J.; Peeters, P.	Getekend door:Jeroen Vercruysse (Signa Getekend op:2025-01-06 16:10:46 +01:0 Reden:Ik keur dit document goed Vlaamse overheid Getekend door:Patrik Peeters (Signature) Getekend op:2025-01-06 16:38:46 +01:0 Reden:Ik keur dit document goed Vlaamse overheid
Project leader:	Verelst, K.	Getekend door:Kristof Verelst (Signature) Getekend op:2025-01-06 16:28:18 +01:0 Reden:Ik keur dit document goed Vlaamse overheid

Approval

Head of Division:	Bellafkih, K.	Getekend door:Abdelkarim Bellafkih (Sig Getekend op:2025-01-07 09:46:50 +01:0 Reden:Ik keur dit document goed Vlaamse overheid

Table of contents

This project has received funding from the Interreg 2 Seas programme 2014-2020 co-funded by the European Regional Development Fund under subsidy contract No [2S07-023]

This project has received funding from the Interreg 2 Seas programme 2014-2020 co-funded by the European Regional Development Fund under subsidy contract No [2S07-023]

INTERREG Polder2C's project

The INTERREG Polder2C's is an international research project within the framework of the updated Sigmaplan for the river Scheldt. The Hedwige-Prosperpolder will be transformed into tidal nature. Depoldering of Hedwige-Prosperpolder offers a unique testing ground, the Living Lab Hedwige-Prosperpolder, for flood defence and emergency response experts. In this environment current and innovative techniques, processes, methods, and products can be tested for practical validation. Thirteen project partners, led by the Dutch Foundation of Applied Water Research (STOWA) and the Flemish Department of Mobility and Public Works (DMOW, Flanders Hydraulics Research), are working together. Together, they aim to improve the 2 Seas regions' capacity to adapt to the challenges caused by climate change.

Flood Defence

The rising sea level is a serious threat to the countries in 2 Seas region. How strong are our current flood defences? What is the impact of environmental elements such as the weather, the presence of vegetation or man-made objects on our flood defences? To answer these questions numerous destructive field tests are carried out in the Living Lab to validate flood defence practices. The project entails in situ testing, guidance on levee maintenance and validation of flood defence infrastructure.

Emergency Response

We aim to improve emergency response by developing the right tools for inspection of water defences, risk evaluation and solutions for flooding. If our water defences do not operate as designed, we must take the right measures to prevent flooding of valuable areas. The Hedwige-Prosperpolder Living Lab offers unique possibilities to exercise emergency management in the event of calamities under controlled but realistic circumstances. Activities that are part of the programme are levee surveillance and monitoring, emergency response exercises, breach initiation and the large European exercise.

Knowledge Infrastructure

We aim to develop a knowledge infrastructure through which existing and new to be developed knowledge will become available and accessible. A necessary success factor for any initiative to improve knowledge is to have its outcomes integrated in practices of a wider community. Knowledge Infrastructure focuses therefore on the consolidation of knowledge acquired in the Living Lab with a variety of activities. Accessibility of data in a user-friendly manner, educational activities in the field and incorporation of knowledge in educational curricula are considered key elements.

Field Station

How can we make sure that both experts in the field and the local public benefit from our project and the learnings about climate change, flood resilience, emergency response and the unique environment of the Hedwige-Prosperpolder? An important and unique way of reaching this goal is realising a Field Station at the project site. It will be used during and after the project for educational purposes, research and as a special meeting place for exclusive occasions.

This project has received funding from the Interreg 2 Seas programme 2014-2020 co-funded by the European Regional Development Fund under subsidy contract No [2S07-023]

1 Introduction

Steady overflow tests

Steady overflow tests on levees, or simply overflow tests (for conciseness), are designed to test the strength of levees and levee covers under the load of a continuously overflowing discharge of water. Within the framework of the INTERREG project Polder2C's, Flanders Hydraulics has designed and built an Overflow Generator (Vercruysse et al., 2023) for this purpose. The Overflow Generator allows to generate a controlled and homogenous discharge of water over the levee crest.

In total 25 overflow tests on Belgian and Dutch levee stretches have been executed during 3 test periods (30/10/2020 to 28/11/2020, 17/02/2021 to 31/03/2021 and 16/11/2021 to 20/12/2021). Different test goals have been addressed to understand the performance of a standard levee cover and to investigate the influence of different anomalies and/or deviations from the 'standard' le^{2}vee cover. The results of the individual tests have been described in Depreiter et al. (2023a, 2023b) and are summarized and discussed in the present report.

Wave overtopping tests

Wave overtopping tests are designed to test strength of levees and their covers under the load of overtopping waves. At the beginning of 2022, INFRAM HYDREN conducted wave overtopping tests with the wave overtopping simulator. The wave overtopping simulator can simulate distributions of wave overtopping. The number and size of the overtopping waves in a test depend on the simulated wave overtopping discharge, the significant wave height and the storm duration.

Different test goals have been addressed to understand the performance of a standard levee cover and to investigate the influence of different anomalies and/or deviations from the 'standard' levee cover. The results of the individual tests have been described in Daamen et al. (2022) and are summarized and discussed in the present report.

This project has received funding from the Interreg 2 Seas programme 2014-2020 co-funded by the European Regional Development Fund under subsidy contract No [2S07-023]

2 Overview

2.1 Scope and location of the overflow experiments

Before the onset of the overflow tests, several test goals were formulated during a workshop in Antwerp on 4th of March 2020. It was identified that the circumstances that could be tested are unlimited. Apart from testing 'pristine', well-maintained levees (as a reference), the initial longlist consisted of items such as testing different environmental conditions (summer/winter, dry/wet), different vegetation conditions (long vegetation, vegetation maintained as default – with Belgian and Dutch differences, short mowed vegetation, desiccated vegetation, different types of vegetation (including flower vegetation), presence of biological anomalies (mice, mole or rabbit burrows, erosion spots at the levee toe due to grazing and resting cattle or sheep) or other discontinuities in the levee cover (e.g. desiccation cracks), transverse transitions (roads on crest of near toe or wall structures), longitudinal transitions (e.g. staircases, edges of concrete constructions), obstacles in the flow path (trees, poles) and damage repair strategies. A selection of this longlist was executed.

Overflow tests have been carried out by Flanders Hydraulics on Belgian and Dutch levees. The individual test setup and results have been described in Depreiter et al. (2023a, 2023b).

Figure 1 - View on an overflow test on a Dutch levee.

2.1.1 Test series goals

For each test, a specific goal was formulated before the start of the test. The first set of tests consisted of 7 tests carried out in October - December of 2020, partly on a Belgian, partly on a Dutch levee stretch:

This project has received funding from the Interreg 2 Seas programme 2014-2020 co-funded by the European Regional Development Fund under subsidy contract No [2S07-023]

- B-OF01 Reference: The first test on a Belgian levee was conducted on a 2 m wide test section with uniform, well-maintained vegetation cover that would serve as a reference. The length of the vegetation is about 20 to 40 cm. An average discharge of 180 L/s.m was applied, for a duration of 21 hours.
- B-OF02 Reference on short grass: Repetition of B-OF01 but with vegetation mowed to a shorter length (10-30 cm), for duration of 18 hours.
- B-OF03 Higher discharge: By narrowing the section to 1 m width, the discharge per meter width was doubled to 360 hours, which ran for 10 hours.
- B-OF04 Tree near toe: The presence of a tree at the levee toe was investigated. The discharge was 160 L/s.m for 1 hour and 27 m.
- B-OF05 Slope erosion due to sheep: An erosion cliff at the toe of the levee was created by sheep grazing on the levee. A discharge of 160 L/s was maintained for 16 hours.
- N-OF01 Reference: The first test on a Dutch levee was conducted at 175 L/s.m for 30.5 hours.
- N-OF05 Large burrow on slope: The presence of an animal burrow halfway the levee slope was investigated at a low discharge of 90 L/s.m.

The second period of testing was conducted in February-March 2021 on Belgian levee sections.

- B-OF06 Reference: A new reference test was conducted and towards the end of the test. Artificial damage was introduced by removing grass patches in a step shape.
- B-OF07 Levee Challenge: Two parallel subsections were damaged and repaired by two student teams before undergoing 3.5 hours of overflow at an average discharge of 180 L/s.m
- B-OF08 Reference: A reference section tested with an increased discharge of 250 L/s.m.
- B-OF09 Reference: A reference section tested with an increased discharge of 375 L/s.m.
- B-OF10 Reference: A reference section tested with an increased discharge of 540 L/s.m by narrowing the section to 1 meter.
- B-OF11 Reference: Testing the impact of a tree near the levee toe at a discharge of 250 L/s.m to see whether scour would develop.

The third and last testing period was also carried out in November-December 2021, with 11 tests executed on a Dutch part of the levee.

- N-OF02 Reference and Clay erosion: A high-discharge test at 550 L/s.m was executed before applying artificial removal of grass to measure the clay erosion process.
- N-OF03 Reference: Reference section for detailed hydraulic measurements at a maximum discharge of 330 L/s.m.
- N-OF04 Reference: Reference section for detailed hydraulic measurements at a maximum discharge of 330 L/s.m.
- N-OF05B Clay infill: After repairing the damaged N-OF05 section with clay infill, the section was retested.
- N-OF05C RTM1: After repairing the damaged N-OF05 section with clay infill and reinforced turf mats, the section was retested.

This project has received funding from the Interreg 2 Seas programme 2014-2020 co-funded by the European Regional Development Fund under subsidy contract No [2S07-023]

- N-OF06 RTM2: The original vegetation of the section was removed and a reinforced turf mat was applied, including hydroseeding. After a season of growth, the section was tested.
- N-OF07 Reference: The original vegetation of the section was removed and a geotextile was applied, and regrowth under the textile was occurring. After a season of growth, the section was tested.
- N-OF08 Grass sods: The original vegetation of the section was removed and replace grass sods were applied. After a season of growth, the section was tested at 200 L/s.m.
- N-OF09 Burrow protection: By means of cover plates, small burrows present in the levee cover where covered before testing the section at a maximum discharge of 500 L/s.m.
- N-OF10 Soft soil reed section 1: A section characterized by the presence of soft soil and a reed patch were tested at a discharge of 200 L/s.m.
- N-OF11 Soft soil reed section 2: A section characterized by the presence of soft soil and a reed patch were tested at a discharge of 200 L/s.m.

The tests can thus be categorized as follows:

- **Hydraulic tests** aiming at better describing and understanding the hydraulics of the overflowing water and the long-duration overflow resistance of the vegetated cover layer. These tests include the following categories:
  - References (i.e., levee sections in a good cover layer state)
  - High discharge (i.e., sections on which the discharge was elevated by narrowing the section width)
- **Damage and erosion tests** aiming at gaining insight in (the influence of surface anomalies on) the strength of the vegetated cover layer. These anomalies are further categorized as follows:
  - Vegetation anomalies
  - Levee profile anomalies
  - Burrows (and burrow protection)
  - Resistance of damage repairs
  - Erosion tests on barren soil (i.e., without vegetation)

The ensemble of all tests may also give insight in the effect of different maintenance strategies between Dutch and Flemish levees.

2.2 Scope and location of the wave overtopping experiments

On the Dutch part of the levee at the Hedwigepolder, 8 wave overtopping tests were commissioned by Flanders Hydraulics at and conducted by INFRAM HYDREN with the wave overtopping simulator in the beginning of 2022 (Figure 2). The tests can be categorized as follows:

- **Hydraulic tests** aiming at better describing and understanding the hydraulics of the overtopping water and the overflow resistance of the vegetated cover layer.
- **Damage tests** aiming at gaining insight on the influence of surface anomalies on the strength of the vegetated cover layer. These anomalies are further categorized as follows:
  - Vegetation anomalies
  - Levee profile anomalies

This project has received funding from the Interreg 2 Seas programme 2014-2020 co-funded by the European Regional Development Fund under subsidy contract No [2S07-023]

- Burrows (and burrow protection)

Because there is no detailed report on these tests *in English*, some details about the individual tests are given below. For a description of all executed wave overtopping test *in Dutch*, including the initial state of the levee cover and damage evolution, one is referred to Daamen et al. (2022).

Figure 2 – The Wave Overtopping Simulator

With the wave overtopping simulator predefined distributions of waves overtopping the crest are generated. The number and size of overtopping waves depend on the average overtopping discharge, the significant wave height, and the storm duration, which in turn are linked with considered storm water levels in the river.

For a description of the test setup, e.g., installed pump capacity, one is referred to Daamen et al. (2022). The test section of a wave overtopping experiment has a width of 4 m, whereas the default section width of the continuous overflow experiments was 2 m.

The following wave overtopping conditions (with corresponding distribution of overtopping waves) were provided by INFRAM HYDREN as modular sets:

I. Water level ~equal to crest level & Hs = 0,5 m (60 l/s per m): 0,5m60lsm
II. Water level 0,2 m above crest & Hs = 0,5 m (60 l/s per m) (~combined wave overtopping & overflow): 0,5m60lsmov
III. Water level ~equal to crest level & Hs = 1 m (190 l/s per m): 1m190lsm
IV. Water level 0,5 m below crest & Hs = 2 m (50 l/s per m): 2m50lsm
V. Water level 2,5 m below crest & Hs = 2 m (100 l/s per m): 2m100lsm.
VI. An optional 6th set of waves (1m50lsm, VI) was also available.

Each 'set' consists of a distinct number of waves each with a certain volume (here ranging from 300 to 3400 l/m), randomly released over the levee (as specified by so-called control files). In general, after each set, more severe loading conditions are applied, until failure occurs. Consecutive sets of waves can be seen as consecutive storm surges the levee cover has to face.

As it is assumed that a storm surge can generate wave overtopping only 1 hour before and 1 hour after high tide, in theory, each set of overtopping conditions is to be generated in a time span of 2 hours. However, wave sets with an average overtopping discharge exceeding the maximum pump capacity, are executed by extending the duration of that set accordingly.

This project has received funding from the Interreg 2 Seas programme 2014-2020 co-funded by the European Regional Development Fund under subsidy contract No [2S07-023]

2.2.1 Test series goals

For each test, a specific goal was formulated before the start of the test.

- N-OT01 Reference (Levee Stretch VI, *teststrook 0* in Daamen et al., 2022): The first test was conducted on a 'test section with a uniform vegetation cover', i.e., well maintained, and would serve as a reference. The length of the vegetation is about 10 cm (which is considered 'short'). Besides some bare spots, molehills are present along the slope. The thickness of the cover layer equals ~70 cm. The slope is 1:2,5.
  The following wave sets were consecutively applied: 0.5m60lsm, 0.5m60lsmov, 1m190lsm, 2m50lsm and 2m100lsm (repeated).
- N-OT02 Wet spot (Levee Stretch VI, *teststrook 1* in Daamen et al., 2022): This test was conducted on a 'test section with a uniform vegetation cover', exempt at the lower part of the slope where a wet spot was present (with bare spots as well). In addition, some mole and mice holes were noticed. The slope is 1:2,5.
  The following wave sets were consecutively applied: 0.5m60lsm, 0.5m60lsmov, 1m190lsm, 2m50lsm and 2m100lsm (partially).
- N-OT03 Animal (+ artificial) holes/burrows (Levee Stretch VI, Teststrook 2 in Daamen et al., 2022): This test was executed on a 'test section with a uniform vegetation cover', but with numerous mole hills in place (as compared to N-OT01). Artificial burrows in the higher and lower part of the slope were drilled. The slope is 1:2,5. The following wave sets were consecutively applied: 0.5m60lsm, 0.5m60lsmov and 1m190lsm (repeated partially and again after creating artificial burrows).
- N-OT04 Artificial holes/burrows (Levee Stretch VI, Teststrook 3 in Daamen et al., 2022): This test was executed on a 'test section with a uniform vegetation cover', with only few bare spots, irregularities, and holes. Artificial burrows in the higher part of the slope were drilled. The slope is 1:2,5.
  The following wave sets were consecutively applied: 0.5m60lsm and 1m190lsm (twice) and after creating artificial burrows followed by 2m50lsm (30') and 1m190lsm (2x 15').
- N-OT05 Bare Clay (Levee Stretch X Kale klei 1 in Daamen et al., 2022): Testing bare clay by removal of the upper ~20 cm of the cover layer over the entire width of the test section, first in the lower, next in the middle and finally in the higher part of the slope, to study clay erosion.
  Consecutive series of regular waves were applied: 100, 200, 350, 500, 700, 1000, 1500, 2000, 2500 & 3000 l/m.
- N-OT06 Bare Clay (Levee Stretch X *Kale klei 2* in Daamen et al., 2022): Testing bare clay by removal of the upper ~20 cm of the cover layer over the entire width of the test section, first in the lower and next in the middle part of the slope, to study clay erosion.
  The following wave sets were consecutively applied: 0.5m60lsm and 1m50lsm.
  In addition, stability of a person facing wave volumes ranging from 200 l/m to 1400 l/m was examined.
- N-OT07 Levee Challenge (Levee Stretch X): 4 (sub)sections were artificially damaged, repaired by students of KULeuven, by Young RWS, by CTW-experts and by DVW within a certain timeframe and subsequently, these repair measures were put to the test.
  The following wave sets were consecutively applied: 0.5m60lsm (1h), 1m50lsm (1h) and 1m190lsm (1h), 2m50lsm (1h), 2m100lsm (1h) and 20 times a 3400 l/m-wave.

This project has received funding from the Interreg 2 Seas programme 2014-2020 co-funded by the European Regional Development Fund under subsidy contract No [2S07-023]

2.3 General properties of the tests

During 3 different test episodes, 25 individual overflow tests have been conducted. A summary of the test conditions and main outcome is shown in Table 1. More details are given in Vercruysse et al. (2023) and Depreiter et al. (2023a, b).

Wave overtopping experiments were first carried out in levee stretch VI, next levee stretch X was tested. Table 2 shows the wave conditions applied. More details are given in Daamen et al. (2022).

Table 1 - Overview of steady overflow test conditions.

Test id	Category	Nominal q ($L.s^{-1}.m^{-1}$)	Width (m)	Duration	Damage outcome?
B-OF01	Hydraulic	180	2	21:00	
B-OF02	Vegetation	180	2	18:00	
B-OF03	Hydraulic	360	1	10:00	
B-OF04	Tree	160	2	1:27	X
B-OF05	Slope anomaly	160	2	16:00	X
B-OF06	Erosion	180	2	19:45	(X artificial)
B-OF07	Special (2x)	180	2	3:27 and 3:30	(X artificial)
B-OF08	Hydraulic / Burrow	250	2	25:30	
B-OF09	Hydraulic	375	2	18:07	
B-OF10	Hydraulic	540	1	2:04	
B-OF11	Hydraulic	250	2	13:02	X
N-OF01	Hydraulic	175	2	30:30	
N-OF02	Hydraulic / Erosion	550	2	10:30	(X artificial)
N-OF03	Hydraulic	330	2	14:30	
N-OF04	Reference	330	2	25:00	
N-OF05	Burrows	90	2	1:19	X
N-OF05B	Repair	375	1	1:15	X
N-OF05C	Repair	150	1	4:30	X
N-OF06	Repair	100	2	2:00	X
N-OF07	Repair	200	2-5	0:30	X
N-OF08	Repair	200	2-5	2:00	X
N-OF09	Burrows	500	2	10:00	
N-OF10	Vegetation	200	2	1:00	X
N-OF11	Vegetation	200	2	0:31	X

This project has received funding from the Interreg 2 Seas programme 2014-2020 co-funded by the European Regional Development Fund under subsidy contract No [2S07-023]

Table 2 - Overview of wave overtopping test conditions.

Test id	Category	Wave condition	Width (m)	Comments Outcome
N-OT01	Reference	I-II-III-IV-V-V	4	After repeating wave set V for 3 hours instant failure occurred.
N-OT02	Wet spot	I-II-II-IV-V*	4	After applying wave set V partially no imminent failure was to be expected.
N-OT03	Animal burrows	I-II-III*-III	4	After applying 3 wave sets (I, II, III) and repeating III partially, artificial burrows were created, and wave set III was again repeated.
N-OT04	Artificial holes	I-III-III-IV*-III*	4	After applying 3 wave sets (I, 2x III), artificial burrows were created, followed by wave sets IV and III partially.
N-OT05	Bare clay	Regular waves	4	Not discussed here.
N-OT06	Bare clay	I & VI + regular waves	4	Not discussed here.
N-OT07	Levee Challenge	I, VI, III, IV, V + regular waves	4	Not discussed here.

This project has received funding from the Interreg 2 Seas programme 2014-2020 co-funded by the European Regional Development Fund under subsidy contract No [2S07-023]

3 Hydraulic insights

3.1 Overflow

3.1.1 Introduction

This section presents an overview of the hydraulic insights gained from the continuous overflow experiments performed within the framework of the Polder2c project. This chapter does not intend to be comprehensive both in the comparison with available literature as in the analysis of the obtained data.

An overview of the hydraulic measurements applied during the continuous overflow tests together with an intercomparison is presented in the Design and application report (Vercruysse et al., 2023). The default measurement setup during the continuous overflow experiments consisted of a discharge measurement, point water level measurement at the crest and at three locations on the landward sided slope and point velocity measurements at three locations on the landward sided slope. The locations at the landward sided slope are named 'upper', 'mobile', and 'lower'. The theoretical locations of respectively the upper, mobile, and lower portal along the slope with respect to the crest was 4 m, 11.8 m and 19.7 m. In reality, there are (sometimes) small deviations. Anyhow, most of the sections have been surveyed with RTK GPS and setup maps of the portals are provided in the factual data reports of each test.

To gain extra insights into hydraulic behaviour of the overflowing water, during some experiments additionally the following measurement techniques are used:

- Particle Tracking Velocimetry (PTV) applied on a floating object and Large-Scale Particle Image Velocimetry (LSPIV) of, a limited area of, the water surface aiming into gaining extra insights into the measured surface velocity,
- a 2D LiDAR to measure the water surface and bottom profile,
- a high-speed camera to record the flow through a transparent side screen, aiming at gaining inside into the vertical flow pattern.

The intercomparison in Vercruysse et al. (2023) leads to the following findings:

- The measurements with the high-speed camera in outdoor conditions proved to be verry challenging and the outcome was not satisfying enough. Therefore, they were not analysed in detail.
- The intercomparison of the point velocity measurements with the PTV and LSPIV measurements let conclude that only at the upper location the point velocity measurements proved to be valuable.
- The LSPIV measurements are only carried out on a limit number of sections and only a limited area was measured.
- Within a certain range of the incident angle the laser beam of the LIDAR partially transmits through the water surface and reflects within the water column or at bottom level, even when the flow is fully aerated.
- The comparison of the LiDAR measurements with the point water level measurement let conclude that depending on the specific location the p95 or the p50 value from the LiDAR measurement seems to be in quite good correspondence with the averaged value of the point water level measurement. Both for the point water level

This project has received funding from the Interreg 2 Seas programme 2014-2020 co-funded by the European Regional Development Fund under subsidy contract No [2S07-023]

measurements as for the LiDAR measurements specific tests are needed to gain a better understanding in what exactly is registered as water level

Based on these findings only the point velocity measurements at the upper location, the PTV measurements of the flow velocity, the point measurement of the water level at the four locations and the p50 and p95 value of the LiDAR measurement are considered for the analysis presented in this chapter. For further details the reader is referred to the design and application report (Vercruysse et al., 2023).

3.1.2 Visual interpretation

Theoretically, the water level at the crest of the levee is equal to the critical water height. Depending on the specific set-up the water level at the crest was equal to the critical water level or even already slightly supercritical. Starting from the crest, at the landward side of the levee, a boundary layer is developing. At the point where this boundary layer reaches the surface, the so-called inception point, aeration starts. The hydraulics of overflow are described in Hewlett *et al.* (1987). The inception point is visible in Figure 3. A literature study on the distance of the inception point to the crest and the water depth at the inception point is presented in Van Cauter (2021). The distance and depth are depending on the slope, roughness length, and the so-called hydraulic roughness Froude number (Keller & Rastogi, 1977):

$$F^* = q/\sqrt{g \cdot sin\theta \cdot {k_s}^3}$$

Where:

- F* Hydraulic roughness Froude number [-]
- q specific discharge [$m^3/s/m$]
- g gravity constant [m/s^2]
- θ slope angle [° or rad]
- k_s hydraulic roughness coefficient for smooth slopes and for stepped slopes k_s = the maximum step height [m]

Figure 3 – Recording taken from the crest visualizing the inception point

This project has received funding from the Interreg 2 Seas programme 2014-2020 co-funded by the European Regional Development Fund under subsidy contract No [2S07-023]

For different discharges, Figure 4 presents the merged images for section B-OF08 from the camera system present at the test section.

Note that the bottom profile is not constant over the channel width, which results in an inception point that is not constant over the section width. On Figure 4 two dashed lines present what could be the start and the end of the area over which the flow becomes self-aerating, the so-called inception point and the point of full aeraetion. At the lowest discharge of 85 L/s/m downstream of the inception point still patches without foam can be noticed, especially towards the left boundary (top boundary on the picture). For a discharge of 175 L/s/m and higher the flow stays aerated after the inception point. Generally, almost no differences are noticeable between the top view of the aerated flow for the discharge of 175 L/s/m and the top view for the flow of 300 L/s/m. At the highest discharge of 375 L/s/m, the inception point is shifted somewhat towards downstream.

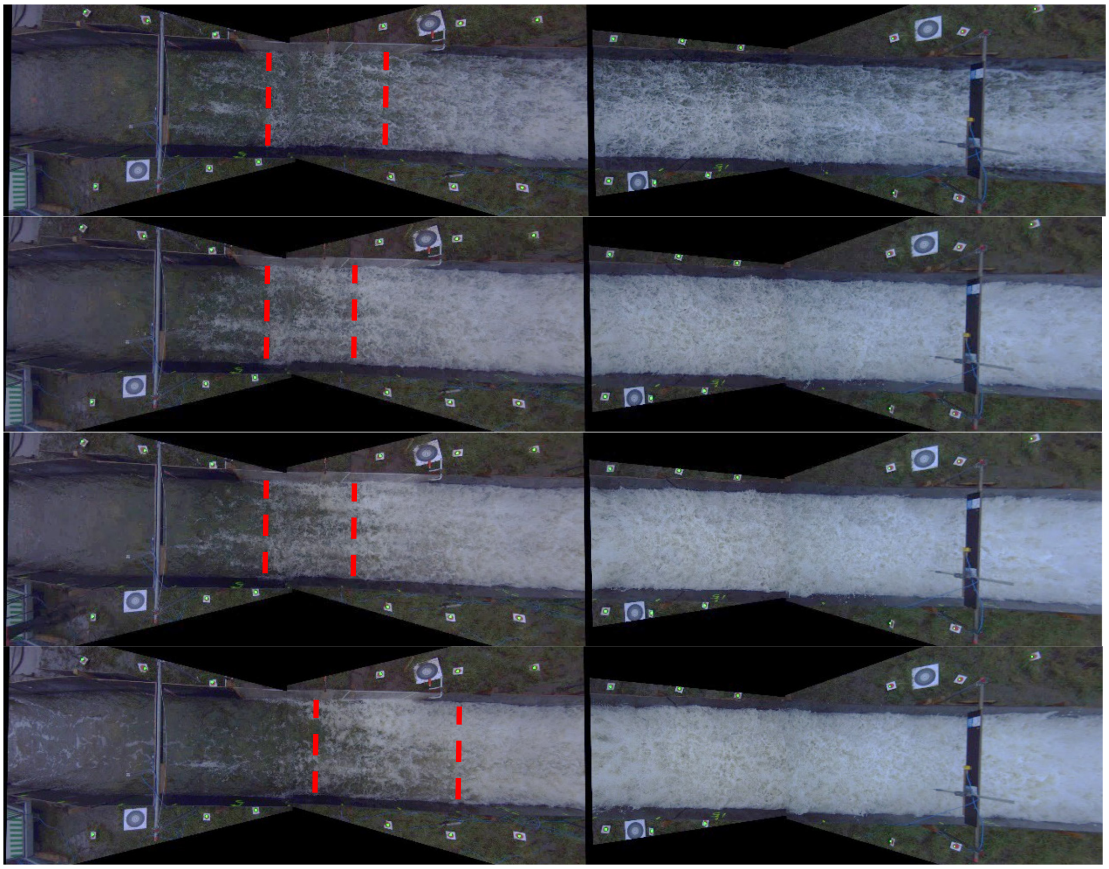

Figure 4 - B-OF08 block 12 top views with varying discharge
(from top to bottom q=85 L/s/m, q=175 L/s/m, q=300 L/s/m, q=375 L/s/m)

3.1.3 Analysis of water height measurements

The variation of the test block averaged measured water height in function of the specific discharge for the locations upper, mobile, and lower is presented in Figure 5. Note that only tests with a constant discharge are considered. During some tests the discharge was varied. For these tests, the test block was split up into smaller blocks with a constant discharge. Note that at the three locations the measured water height increases with increasing discharge.

This project has received funding from the Interreg 2 Seas programme 2014-2020 co-funded by the European Regional Development Fund under subsidy contract No [2S07-023]

There is a considerable spread on the results but for a given section the measurements seem to be more coherent. Generally, an increasing water height from location upper towards location mobile can be noticed. From location mobile towards location lower there is no clear trend.

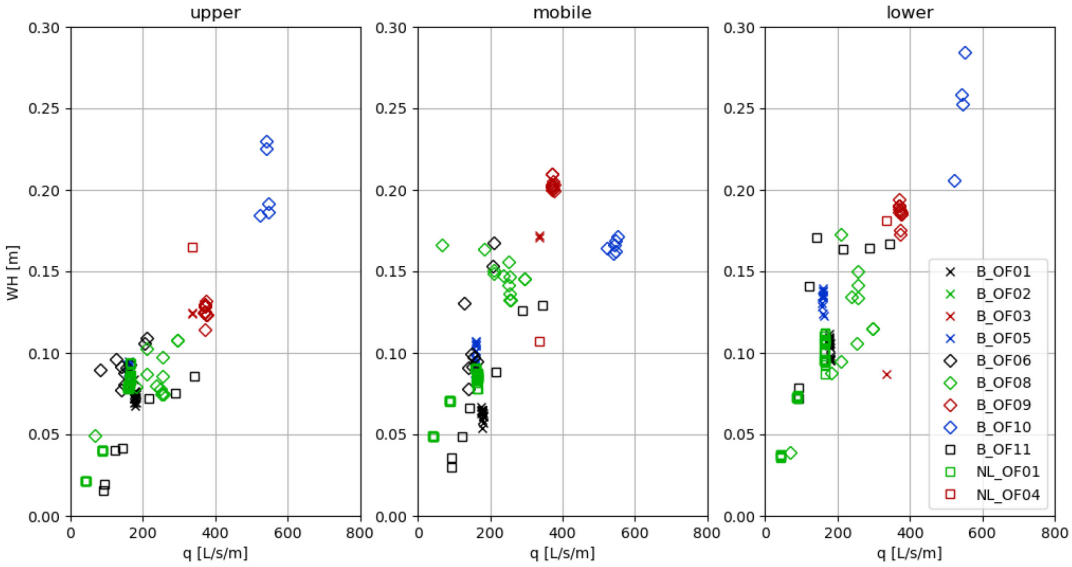

Figure 5- Variation of water height in function of discharge for locations upper, mobile, and lower (i.e., upper, mobile, and lower slope)

Additional water level measurements were performed using a 2D LiDAR. For the hydraulic analysis in this report the LiDAR measurements performed within the framework of the Master Thesis of Van Cauter (2021) are used. The LIDAR measurements were carried out at section B-OF8 during flow block 10 and flow block 12. During flow block 10 the LiDAR was mounted at the lower camera portal and during block 12 at the upper camera portal.

First an analysis of the bottom profile measured during both flow blocks was carried out. The bottom profile was measured with LIDAR at the end of the overflow event. The zones with blanking due to the measurement portals are filtered out. For visualization purposes the x-axis is aligned with the slope and the zero is shifted towards the transition from the crest towards the slope. The measured bottom profile for flow block 10 and flow block 12 are visually aligned. Figure 6 presents a comparison of the measurement of the bottom profile for these 2 flow blocks. Note that there is generally a good agreement between both measurements. The transect measured with the LIDAR at the lower portal was not exactly aligned with the transect measured with the LIDAR at the upper portal. This could explain some local differences between the two measured bottom profiles.

This project has received funding from the Interreg 2 Seas programme 2014-2020 co-funded by the European Regional Development Fund under subsidy contract No [2S07-023]

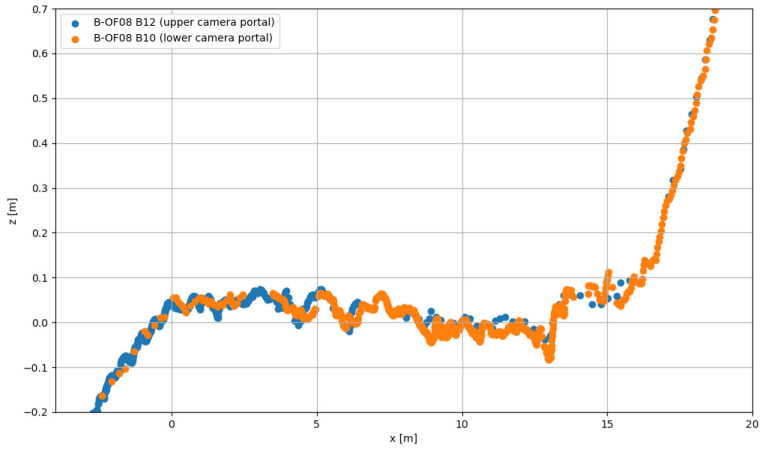

Figure 6 – 2D LiDAR measurement bottom

Next the LiDAR measurements during overflow are processed. The processing of the data involves, analogue as for the measurement of the bottom level, the filtering of the reflections of the measurement portals and performing an orthogonal projection.
The size of the zones with partially blanking caused by the smaller measurement portals increases, see Figure 7. Also, these zones are manually selected and filtered out.

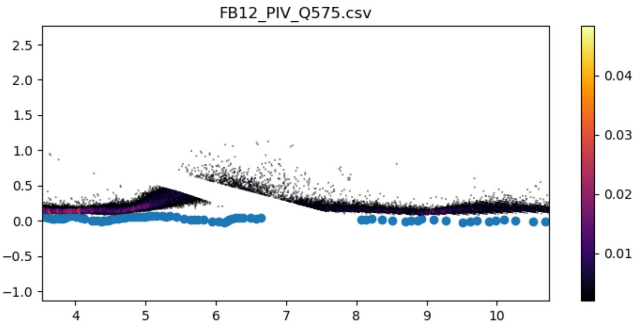

Figure 7 – Blanking zone due to one of the smaller measurement portals. The black dots represent the water surface reflections, the blue dots are the ground reflections (measured without overflow).

The LiDAR measurements during flow block 10 and flow block 12 are carried out for different discharges. The measurements of the LIDAR are not synchronized with the measurements of the Data Acquisition system. The time stamp of the measurement at different discharges is noted in the logbook. The aimed discharge during the 2D LiDAR measurements is also presented in the filename. A comparison between the measured discharge at the time of the LIDAR-measurements and the aimed discharge derived from the filename reveals a good agreement, but sometimes some discrepancies are present. Therefore, the discharge for the analysis of the LIDAR-measurements is derived from the filename, being the aimed discharge. The results are presented in Figure 8 for flow block 10 with the LiDAR on the lower camera portal, and in Figure 9 for flow block 12 with the LiDAR on the upper camera portal. As noted in paragraph 3.1.1 further research is needed on the LiDAR measurement. When compared to

This project has received funding from the Interreg 2 Seas programme 2014-2020 co-funded by the European Regional Development Fund under subsidy contract No [2S07-023]

the mean value of the ultrasonic measurement at some locations there was a good correspondence with the p50 value from the LiDAR while at other locations there was of good correspondence with the p95 value, see the design and application report for details. For this reason, both the p50 as the p95 value are presented in Figure 8 and Figure 9.

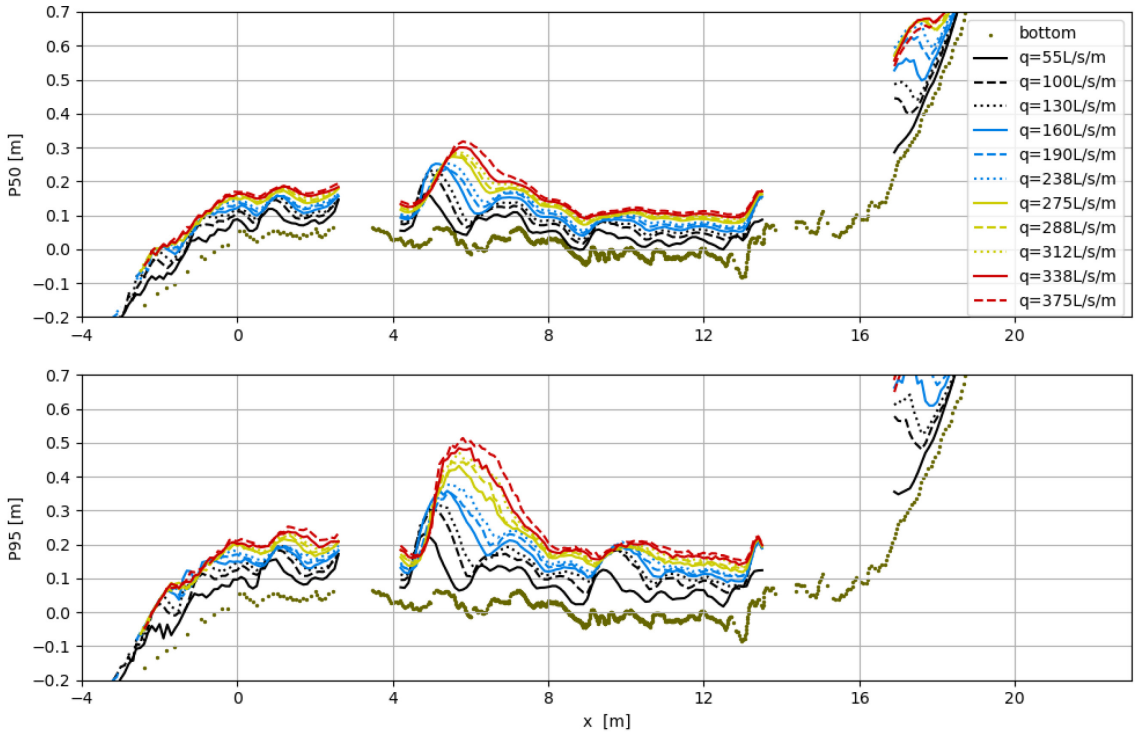

Figure 8 – Results LiDAR measurement B-OF08-B10 (Lidar mounted on lower camera portal)

This project has received funding from the Interreg 2 Seas programme 2014-2020 co-funded by the European Regional Development Fund under subsidy contract No [2S07-023]

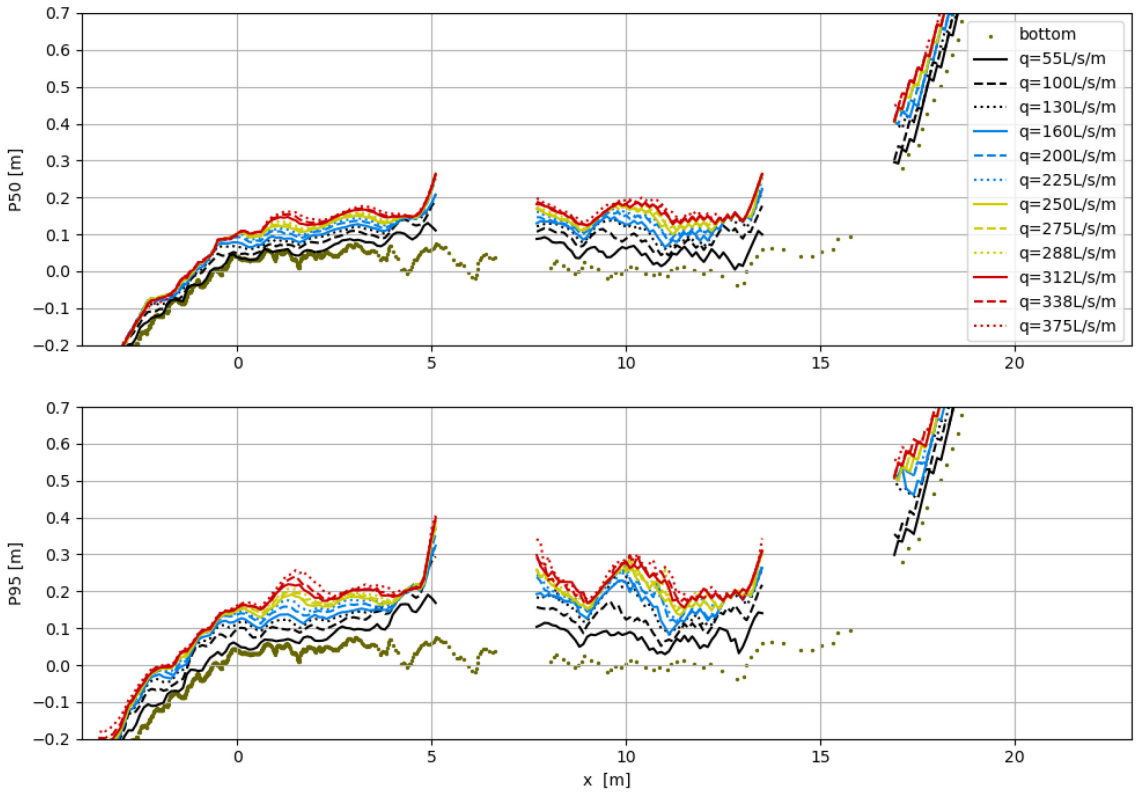

Figure 9 - Results LiDAR measurement B-OF08-B12 (LiDAR mounted on upper camera portal)

Figure 8 compares for some specific discharges the water level measured during flow block 10 with the water level measured during flow block 12.

This project has received funding from the Interreg 2 Seas programme 2014-2020 co-funded by the European Regional Development Fund under subsidy contract No [2S07-023]

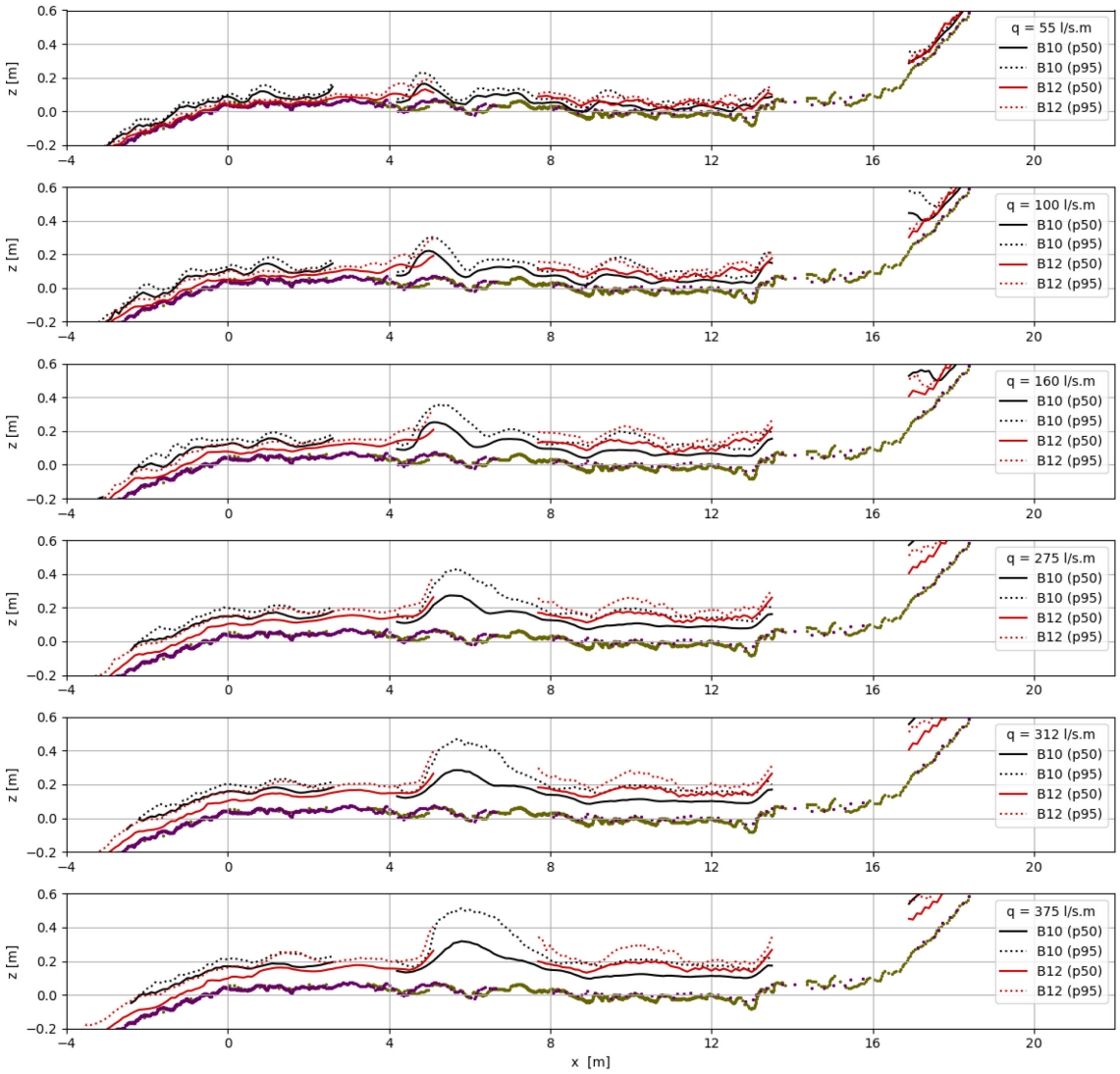

Figure 10 – Lidar water height measurement B-OF08 for different discharges

Some differences are noticed between flow block 10 and flow block 12. During the validation of flow block 12 it was noticed that within a range of incident angles the LiDAR beams penetrate partially through the water surface and reflect within the water column or at the bottom level. This could explain the lower values measured during flow block 12 at the upper part of the slope. This difference is higher for the p50 values then for the p95 values. Also no clear transition a few meters downstream of the crest, indicating the inception point, is present. Van Cauter (2021) studied this phenomenon in depth and concluded that only considering LiDAR measurements is insufficient to determine the location of the inception point. This is somewhat counterintuitive with the clear transition that can be noticed in the recordings of the water surface at the inception point, see Figure 3 in paragraph 2.1. At approximately 5 m a clear rise in the measured water height is noticed. The bottom profile shows a local depression immediately before this point. A recording of the water surface during different discharges of flow block 12 of test B-OF08 is presented in Figure 4. At the middle of the image there seems to be an increase at the right outer boundary. Note that a cross reference of the LiDAR and the images of the camera system could not be carried out and that the exact

This project has received funding from the Interreg 2 Seas programme 2014-2020 co-funded by the European Regional Development Fund under subsidy contract No [2S07-023]

location of the LiDAR line over the width of the test section was also not registered in the logbook. Van Cauter (2021) describes also a local depression followed by an increase of the water depth, a phenomenon that is not covering the full width of the section which is in correspondence with the visual interpretation of Figure 4. A direct comparison with the results described in Van Cauter (2021) is hampered because of the use of another reference system. Further research is recommended to compare the results of the LiDAR measurements with the camera recordings of the water surface, the notes in the logbook, additional recordings and the insights presented in Van Cauter (2021).

3.1.4 Analysis of velocity measurements

The analysis presented in the Design and application report let conclude that only the point velocity measurement at location upper is valuable. The point velocity and the section averaged velocity (=q/WH) at location upper is presented in Figure 11. Location upper is positioned at approximately 4 m from the crest and is situated upstream of the inception point with accelerating, but not yet aerated low. In these conditions the electromagnetic point velocity measurement should conduct reliable measurements. Because of the flow still being accelerated, the exact location with respect to the crest and the initial velocity on the crest will have an important influence on the velocity at the location upper. Consequently, the velocities presented in Figure 11 can therefore not be used for an intercomparison of the velocity at location upper for different test sections. For a particular test section an increase in specific discharge results in an increase in velocity. The maximum measured velocity at location upper is equal to 3.7 m/s for the point velocity measurement and is equal to 4.0 m/s for the section averaged velocity. Note that these maximum velocities are not measured on the same test section. Comparing the point velocity measurement with the section averaged velocity it is noted that no relationship between these two velocity measurements is present.

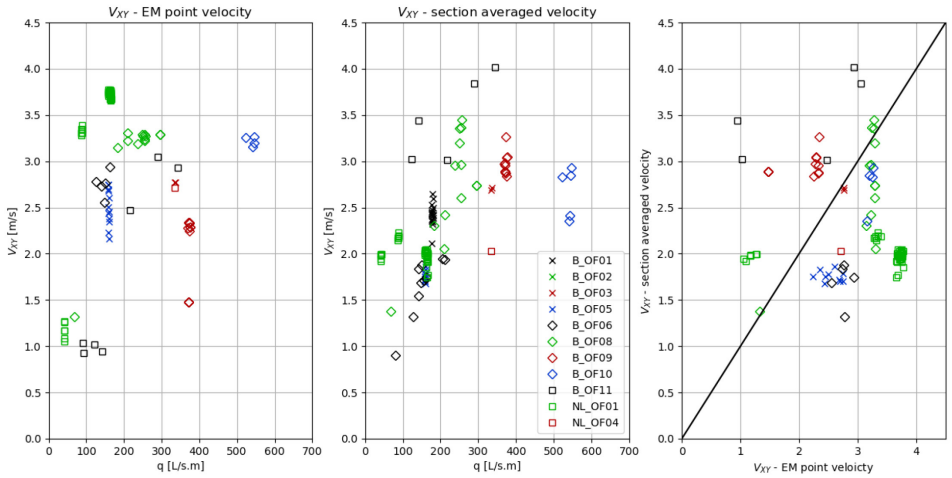

Figure 11 – Time averaged point and section averaged velocity at location upper

During some tests a velocity profile along the slope was measured using PTV. The PTV measurements were performed on merged images from the four cameras of the camera system and projected on an average plane through the reference points. At the crest and toe of the levee the bottom starts to deviate from this plane and consequently also the velocity. The zero point of the x-axis corresponds to the transition from the crest towards the slope.

This project has received funding from the Interreg 2 Seas programme 2014-2020 co-funded by the European Regional Development Fund under subsidy contract No [2S07-023]

Figure 12 presents the variation of the velocity over the landward levee slope for different discharges during test B-OF08.

The results shows an increase in velocity towards what visually seems to be an equilibrium velocity. For the smallest discharge of approximately 60 L/s/m a steep increase over approximately the first 2 m is noticed towards an equilibrium velocity of approximately 3 m/s. For the higher discharges, 174 L/s/m until 388 L/s/m, the differences in variation of the velocity is smaller. An increase in discharge seems to result in only a slight increase in velocity. The maximum velocities for discharges 175 L/s/m till 375 L/s/m are in the order of 5 m/s until 6.5 m/s.

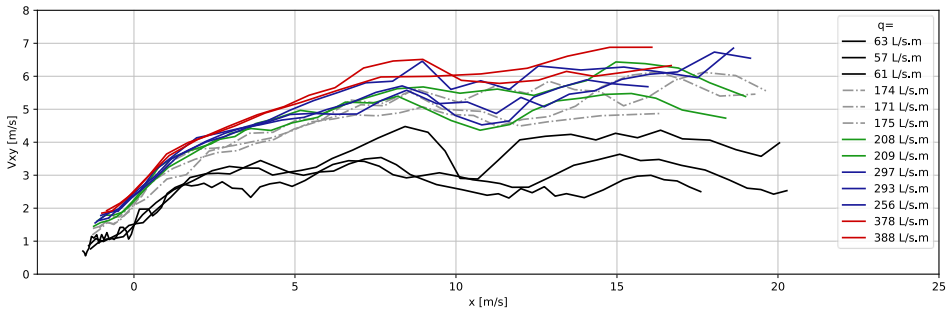

Figure 12 – PTV measurement B-OF08

The result of the PTV measurement on test section NL-OF03 and test section NL-OF04 are presented in Figure 12. Note that during the tests performed on test sections NL-OF03 and NL-OF04 the discharge meter was not working properly and the outflow out of the overflow generator was not properly dissipated, see the design and application report for details. The specific discharges are therefore calculated from the pump propeller rotation conversion presented in the design and application report. The camera orientation was somewhat less optimal resulting in a smaller reach compared with the PTV measurements on test section B-OF08.

The velocity profiles for different discharges during tests N-OF03 and N-OF04 are presented in

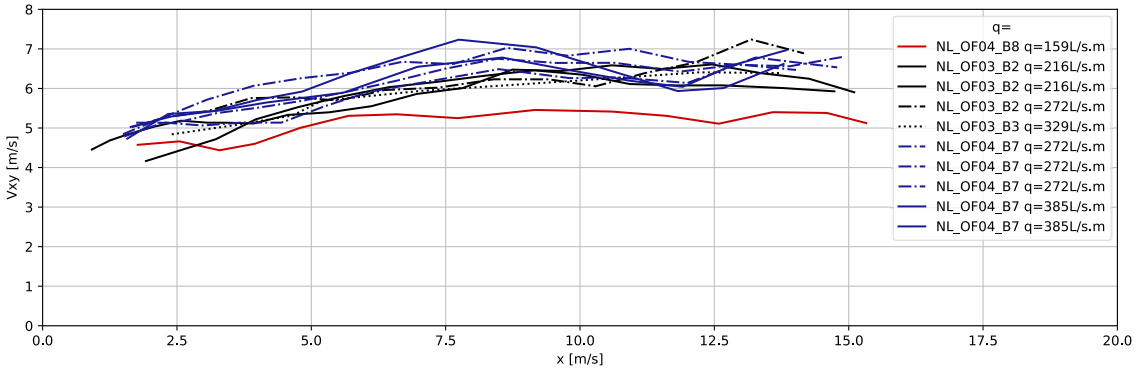

Figure 13. Note that at 7.5 m downstream of the crest the equilibrium velocity seems to be reached. For the discharges between 216 L/s/m and 395 L/s/m equilibrium velocities between 6 m/s and 7 m/s are measured, only for the lowest discharge of 160 L/s/m a lower equilibrium velocity in between 5.0 m/s and 5.5 m/s is measured. The velocity at 2.5 m distance from the crest varies between 4.0 m/s and 5.0 m/s, being somewhat higher than the velocity between

This project has received funding from the Interreg 2 Seas programme 2014-2020 co-funded by the European Regional Development Fund under subsidy contract No [2S07-023]

3.5 m/s and 4.5 m/s measured at test section B-OF08. A possible explanation could be the insufficient dissipation of the outflow out of the generator during the tests N-OF03 and N-OF04 resulting in a higher starting velocity at the beginning of the slope. Unfortunately, the images start at 2.5 m downstream of the crest so this hypothesis could not be verified using the PTV measurements.

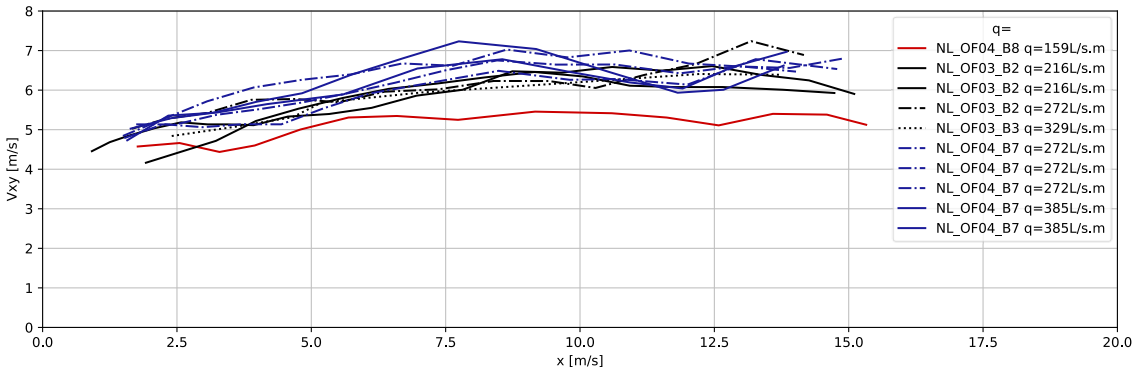

Figure 13 – PTV measurement NL-OF03

For supercritical flow over vegetated slopes the equilibrium velocity is calculated based on the hydraulic grade line theory using the following formula

$$V_{eq} = \frac{R^{\frac{2}{3}} S_0^{\frac{1}{2}}}{n}$$

$$V_{eq} = \left(\frac{S_0^{\frac{1}{2}}}{n}\right)^{3/5} \cdot q^{2/5}$$

Where:

- V_{eq} Equilibrium velocity [m/s]
- R Hydraulic radius [m]
- S_0 Bed slope defined as sin θ [-]
- n Gauckler-Manning coefficient [$s/m^{1/3}$]
- q Specific discharge [$m^3/s/m$]

Concerning the roughness value for a vegetated slope, the CIRIA manual (Hewlett *et al.*, 1987) presents three different flow regimes in function of the hydraulic loading (see Figure 3.13).

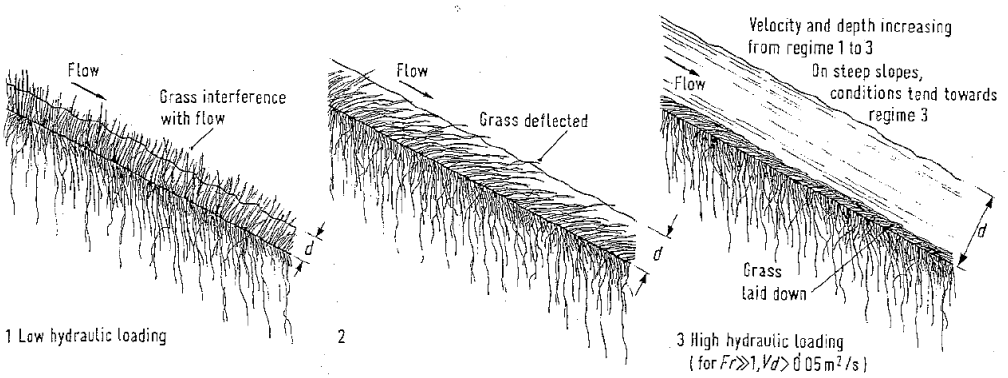

Figure 3.14. Effect of hydraulic loading on grassed surface (Hewlett *et al.*, 1987)

This project has received funding from the Interreg 2 Seas programme 2014-2020 co-funded by the European Regional Development Fund under subsidy contract No [2S07-023]

For flow type 3 the Froude number is noticeable higher than 1 and the so-called flow parameter should be higher ten 0.05 m^2/s. The flow parameter (V x R) is defined as the velocity multiplied by the hydraulic radius or depth for an infinite wide channel. Figure 15 presents for the different continuous overflow test the value of the Froude number and the flow parameter calculated using the point measurement of water level and velocity at location upper. Note that for these calculations the test section is considered as an infinite wide channel due to the smooth side boundaries of the test section. The Froude numbers at location upper are within the range 1.5 till 5.5 and with a few exceptions the flow parameter is above 0.05 m^2/s. Consequently, the flow can be considered as type 3 flow.

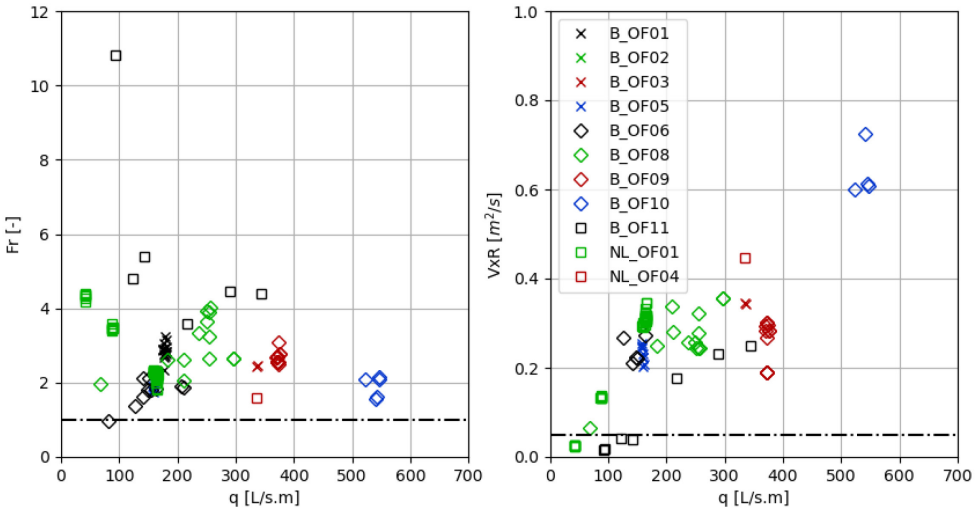

Figure 15 – Froude number and flow parameter and flow 3 regime limit (dashed lines) at location upper

For slopes flatter than 1 on 10 the CIRIA manual recommends to determine the manning coefficients based on the flow parameter method developed by the US Department of Agriculture Stillwater Laboratory in Oklahoma (Cox, 1942; Palmer, 1945; Ree & Palmer, 1949). For slopes 1 on 3 and steeper and a discharge exceeding 50 L/s/m a manning coefficient 0.02 $s/m^{1/3}$ is recommended. Note that the landward sided slope is just below 1/3 and that except from a few short tests with a very low discharge the discharge exceeds 50 L/s/m. Based on the CIRIA manual a Gauckler-Manning coefficient equal to 0.020 $s/m^{1/3}$ is applied as a first assumption.

Using this hydraulic roughness, for the specific discharges measured at sections with PTV-measurements available, i.e., test sections B-OF08, N-OF03 and N-OF04, the equilibrium velocity is calculated. The factual data reports of these test sections mention a slope of 19° for test section B-OF08 and a slope of 22° for sections N-OF03 and N-OF04. Using this slope and a manning roughness coefficient equal to 0.020 $s/m^{1/3}$ the variation of the equilibrium velocity in function of the specific discharge of the test is calculated and plotted in Figure 16 using a blue line. From the PTV measurements the equilibrium velocity can be derived as the average value of the velocity between 10 m from the crest and the end of the measurement range. Also, these velocities calculated form the PTV measurements are plotted on the graphs using

This project has received funding from the Interreg 2 Seas programme 2014-2020 co-funded by the European Regional Development Fund under subsidy contract No [2S07-023]

blue dots. Figure 15 shows that the equilibrium velocity calculated using the formula above, as well as for test section B-OF08 as for both test sections N-OF03 and N-OF04, is significantly lower than the equilibrium velocity derived from the PTV-measurements. Subsequently by linear regression on the graphs presenting the variation of the velocity as a function of the specific discharge to the power 2.5 a new value for the Gauckler-Manning coefficient is derived. The outcome from this linear regression is a Gauckler-Manning coefficient equal to 0.0128 s/m$^{1/3}$ for sections B-OF8 and equal to 0.0121 s/m$^{1/3}$ for sections N-OF3 and N-OF4. Note that there is good correspondence between the two different test sections. However, the calculated Gauckler-Manning coefficient is considerably lower than the 0.020 s/m$^{1/3}$ recommended by CIRIA and compared with literature values. For example a Gauckler-Manning coefficient of 0.013 s/m$^{1/3}$ corresponds with trowel finished concrete (Chow, 1959).

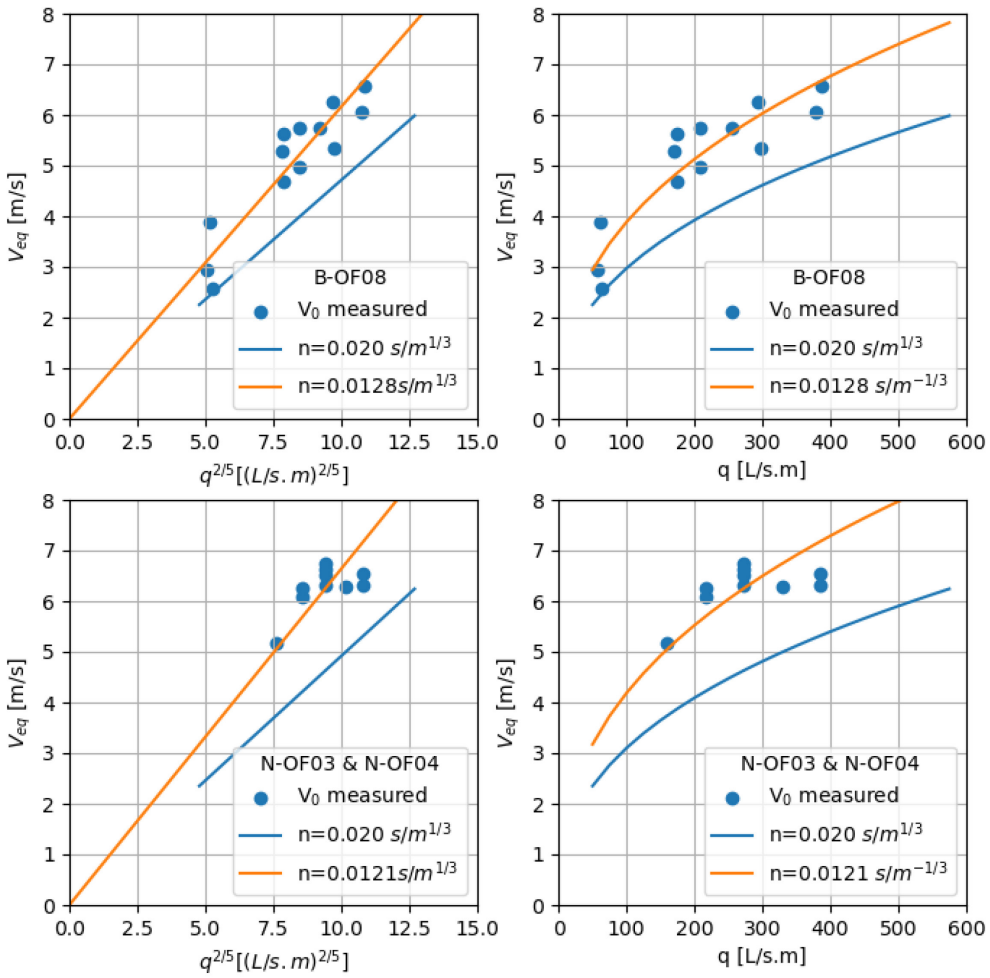

Figure 16 – Equilibrium velocity in function of specific discharge (n= 0.020 s/m$^{1/3}$)

Note that the velocities measured by PTV exceeds the expected velocities. The presumable explanation is that the particles used for PTV were floating at the surface where the velocity will be higher than the section averaged velocity. The calculated Gauckler-Manning coefficient based on the by PTV measurements derived velocities corresponds with a value for trowel finished concrete. The equilibrium velocity based on the calibrated Gauckler-Manning coefficient exceeds the equilibrium velocity based on the Gauckler-Manning coefficient

This project has received funding from the Interreg 2 Seas programme 2014-2020 co-funded by the European Regional Development Fund under subsidy contract No [2S07-023]

recommended by CIRIA with 31 % for B-OF08 and 35 % for NL-OF03. Little information is known on the velocity profile and aeration concentration in overflow conditions over a levee. The flow could be comparable with the flow pattern over a stepped chute (Chanson, 2002). Van Cauter (2021) presents a literature review and the definition of an equivalent pseudo bottom.

The goal was to gain more insight in the flow profile and aeration concentration by combining the high-speed recordings and the LiDAR measurements. Unfortunately, the high-speed recordings were not successful. Further research is recommended to gain insights in the hydraulics during overflow.

For the erosion resistance presented in §4.1 the velocity measured by the electromagnetic point velocity meter at location upper will be used. Note that these values will be an underestimation for the velocities further on the slope.

3.1.5 Discharge – overflow height

During the overflow test the main parameter was the supplied discharge to the test section. However, during real overflow events the main parameter is the height of the water level above the crest of the levee. The overflow discharge is then resulting from the height of the water level above the crest of the levee. The water height above the crest is defined as the difference between the water level at the river and the crest level. To calculate the specific discharge for an overflow event the formula for a broad crested weir is used:

$$q = C_D \cdot (H_{river} - H_{crest})^{3/2}$$

Where:

- q — Specific Discharge — [$m^3/s/m$]
- Cd — Discharge coefficient — [$m^{1/2}/s$]
- H_{river} — Water height in the river with respect to the local datum — [m]
- H_{crest} — Crest height with respect to the local datum — [m]

The international Levee Handbook (CIRIA, 2013) presents following formula from Henderson (1966) to calculate the specific discharge:

$$q = 0.553 \cdot \sqrt{g} \cdot (H_{river} - H_{crest})^{3/2} = 1.73 \cdot (H_{river} - H_{crest})^{3/2}$$

At Flanders Hydraulics (FH) in the past a similar formula is used with a weir coefficient C_D equals to 1.36. This coefficient was based on a calibration for the flood control areas within a 1D model of the Sigmaplan in Belgium (Laforce *et al.*, 1990). In the early days FH executed overflow tests on physical models (Bonnet & Lamoen, 1937). Both discharge and water level above the crest are reported from these tests. Based on these data the discharge coefficients presented in Figure 17 are derived. For the experiments with the cement lining there is a clear increase in discharge coefficient with increasing water height above the crest, while for the grass covering a rather constant higher discharge coefficient is derived.

This project has received funding from the Interreg 2 Seas programme 2014-2020 co-funded by the European Regional Development Fund under subsidy contract No [2S07-023]

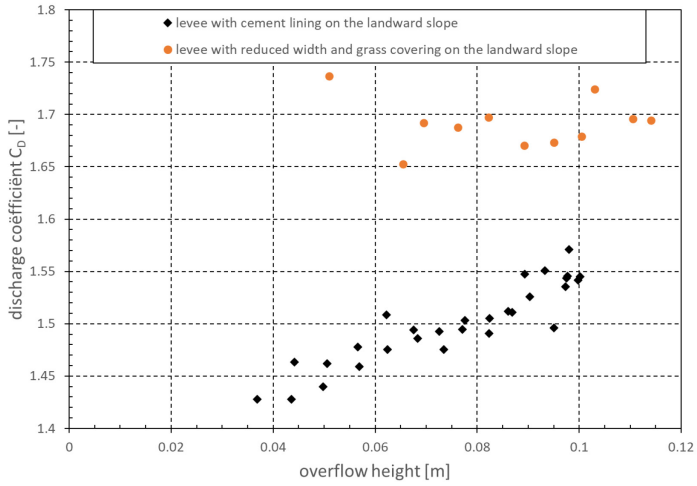

Figure 17 – Discharge coefficient derived from (Bonnet & Lamoen, 1937).

Discharge coefficients for overflow over an embankment are presented in Schall *et al.* (2012). The discharge coefficient varies with overflow height, the ratio overflow height to crest length, the embankment covering and the submergence factor. For an overflow height of 0.3 m and a crest width 2 m the ratio is 0.15 m. For a ratio overflow to crest height equal or lower than 0.15 and non-submerged flow the discharge coefficient in relation to the overflow height and the embankment covering (paved or gravel) is presented in Figure 18. For the overflow experiments the overflow height is in the range 0.15 m to 0.40 m. The discharge coefficient of gravel embankment equals 1.45 for an overflow height 0.15 m and increase to 1.59 for an overflow height 0.40 m. Note that for higher overflow heights or a smoother embankment covering the discharge coefficient increase to approximately 1.68.

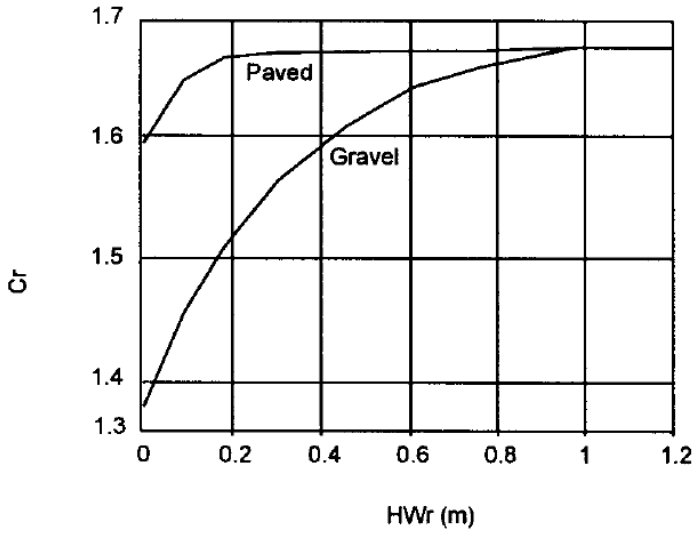

Figure 18 - Discharge coefficient in function of overflow height (Schall *et al.*, 2012)

For a broad crested weir with an upstream sided slope equal to 1:2 and a downstream sided slope within the range 1:5 and 1:1 Tracy (1957) present discharge coefficients based on Bazin (1896). The discharge coefficient is presented as a function of the ratio water level above the crest-to-crest length. For a ratio overflow to crest length below 0.20, which is the case for the

This project has received funding from the Interreg 2 Seas programme 2014-2020 co-funded by the European Regional Development Fund under subsidy contract No [2S07-023]

overflow heights tested at Polders2c's the discharge coefficient is constant and independent of the downstream slope. From the figure presented in the report a discharge coefficient C_D equal to 1.61 is derived.

Azimi & Rajaratnam (2009) propose empirically determined formulations for the discharge coefficient based on a large data set of physical experiments with broad crested weirs using weir height, water height in river, rounding and crest width as variables. When comparing the data set-up with the overflow conditions of a levee during overflow it is concluded that the water height above the crest considered for the Polder2C's tests is at the lower end of the available spectrum. This means that fewer data points are available and local effects as roughness and small variations in height become more important. When compared with the results for a wide spillway with rounded corners, a flow coefficient between 1.21 and 1.56 is found for the relevant range of crest width, spillway height and water level height from the scale model experiments.

It is concluded that for a given water level above the crest the discharge is depending on the river and landward sided slope of the levee, the smoothness and hydraulic roughness of the crest, the ratio of water level above the crest-to-crest length and the velocity component of the water in the river. Most studies carried out use broad crested weirs or consider overflow over embankments. From the limited literature review only limited experimental data was found applicable to levee overflow. The flood control areas constructed along the river Scheldt and its tributaries are filled by overflow over lowered levees. It's recommended to check if based on topographic data and water level measurements at river and flood control area side a value for the discharge coefficient as a function of the overflow height can be determined.

Considered a range for the discharge coefficient from 1.36 (current value in use at FH for overflow levees) till 1.73 (recommended by the international levee handbook) the relation of the specific discharge in function of water level above the crest presented in Figure 19 is obtained.

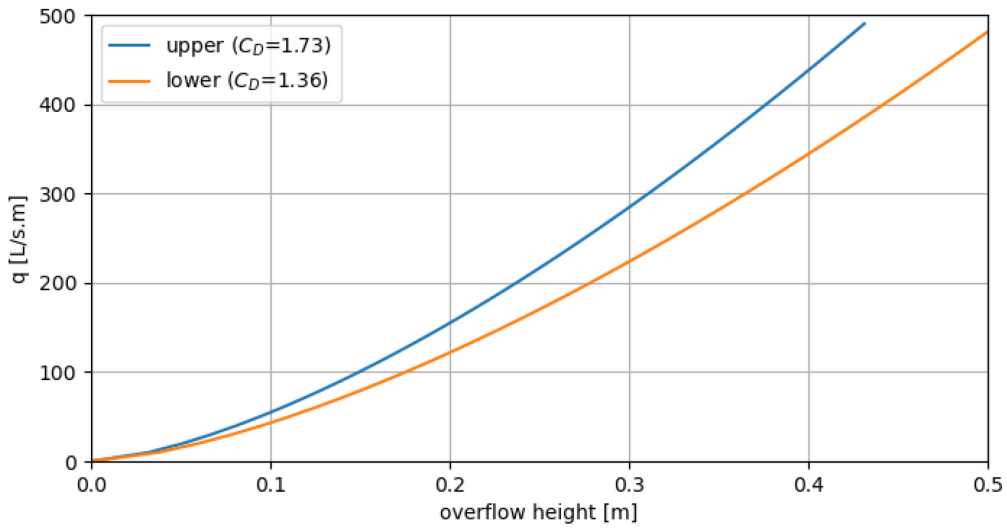

Figure 19 – Specific discharge in function of overflow height

This project has received funding from the Interreg 2 Seas programme 2014-2020 co-funded by the European Regional Development Fund under subsidy contract No [2S07-023]

3.2 Wave overtopping front velocities

3.2.1 Introduction

Van der Meer et al. (2010) derived the following equation to estimate the wave front (depth-averaged) velocity (u_b) at the crest given the wave volume (V):

$$u_b = 5\ V^{0,34}$$

Where:

- u_b wave front (depth-averaged) velocity [m/s]
- V Wave volume [m^3]

Wave front velocities were measured by INFRAM HYDREN along the slope for predefined overtopping volumes, ranging from 300 l/m to 3400 l/m, using so-called action cams (Daamen et al., 2022).

3.2.2 Overview of estimated front velocities at N-OT01

Table 3 and Figure 20 show wave front velocities for different wave volumes. The calculated and measured front velocities are of the same order of magnitude. Following the measurements, front velocities tend to increase along the upper part of the slope and decrease again along the lower part. For a detailed description of wave overtopping hydraulics, one is referred to Hughes (2008).

Table 3 – Wave front velocities on crest (calculated) and along slope (measured)

Wave volume (V)	At crest	Along slope: upper	Along slope: mid	Along slope: lower
(l/m)	(m/s)	(m/s)	(m/s)	(m/s)
300	3,3	4,1	5,0	4,7
350	3,5	4,0	4,7	4,9
400	3,7	4,5	4,9	4,8
450	3,8	4,1	4,8	5,1
500	4,0	3,4	4,8	4,6
600	4,2	3,7	4,5	4,7
700	4,4	4,1	4,9	4,9
800	4,6	4,2	5,2	5,5
1000	5,0	4,7	5,4	5,5
1250	5,4	4,9	5,1	5,4
1500	5,7	4,7	5,5	5,3
1750	6,0	5,6	5,8	5,0
2000	6,3	5,7	6,6	5,5
2500	6,8	5,9	7,1	6,1
3000	7,3	6,2	7,7	6,4
3400	7,6	6,1	7,5	5,7

This project has received funding from the Interreg 2 Seas programme 2014-2020 co-funded by the European Regional Development Fund under subsidy contract No [2S07-023]

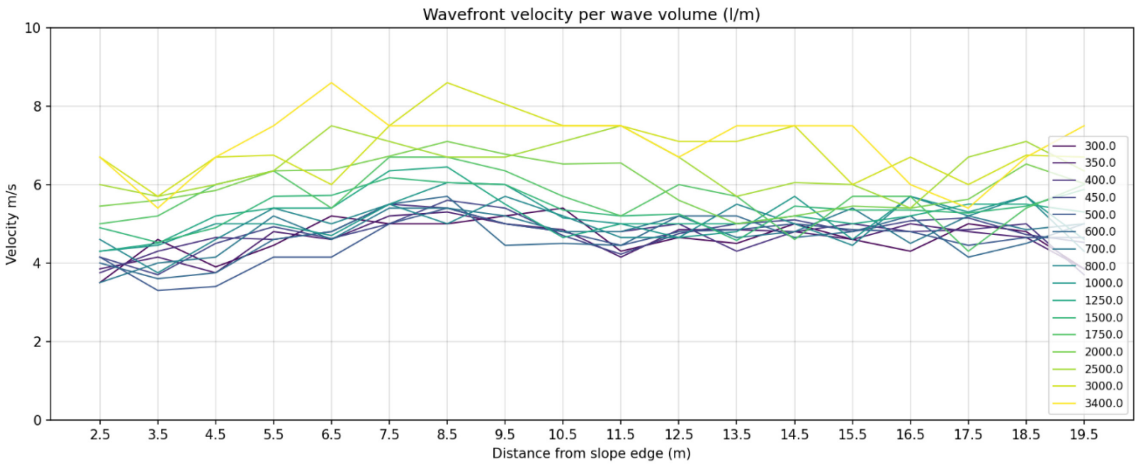

Figure 20 – Measured wave front velocities along the slope

This project has received funding from the Interreg 2 Seas programme 2014-2020 co-funded by the European Regional Development Fund under subsidy contract No [2S07-023]

4 Insights from overflow tests

During the Polder2C's project, 25 overflow tests have been conducted. An overview of the setup is given by Vercruysse et al. (2023) and published in Koelewijn et al. (2022). Some of these experiments led to significant damage and termination of the experiment in order not to critically damage the levee. However, several tests have been terminated without any serious damage occurring.

In this chapter, first the erosion resistance of the grass cover layer is described (§4.1). The evolution of the cover layer state was similar for most of these experiments. In §4.2 the evolution of the cover layer state description is based on the observations described in Depreiter et al. (2023a, b). Then the effects of anomalies on the levee slope (paragraph 4.3) and the influence of alternative vegetation (paragraph 4.3) are discussed.

4.1 Erosion resistance of the grass cover layer

Erosion tests on grass covered hydraulic infrastructure has been subject of studies for decades, but the application of steady overflow tests (in contrast to other types of tests such as the wave overtopping tests), have not (widely) been conducted in Flanders and the Netherlands. A classical reference is the grass cover strength graph expressing a relation between flow duration, limiting flow velocity and grass cover quality (CIRIA 1976; CIRIA, 1987). For the overflow tests conducted within the framework of the Polder2C's project, the experiment duration and average velocity recorded or calculated[1] at the upper slope have been plotted on top of these graphs. This comparison is presented in Figure 21. Several observations can be made from this graph:

- The average velocity recorded at the upper slope sensor position, is mostly situated between 2 and 3 m/s. As shown in Vercruysse et al. (2023), and discussed in §3.1.4, there is uncertainty about the electromagnetic velocity measurements under aerated conditions. Because the measurements at the upper slope are often less or even not aerated, the quality of these data is most reliable. The same type of measurements lower on the slope are not reliable enough but is known to be higher than depicted here. PTV measurements have been performed on selected overflow tests and indicated accelerating flows from 2-3 m/s at the upper slope, up to 4-6 m/s at the lower slope. In this sense, the velocity of the data points is higher than shown hereunder. The consequence of this will be discussed below.
- There is a cluster of data points with short experiment duration (< 2 hours). These are experiments aiming specifically at testing slope anomalies although the reason of failure was not always as anticipated. It appeared that burrows and barren or soft soil areas were most vulnerable.
- There is a wide cluster of data points that did not lead to significant damage or further failure of the levee. These tests have durations of 4 to 30 hours.
- Two tests led to failure after 10 to 20 hours. The presence of burrows and/or other biological activity was related to the weakening of the levee cover (see §4.3).

[1] *Discharge per unit width divided by the water height at that location.*

This project has received funding from the Interreg 2 Seas programme 2014-2020 co-funded by the European Regional Development Fund under subsidy contract No [2S07-023]

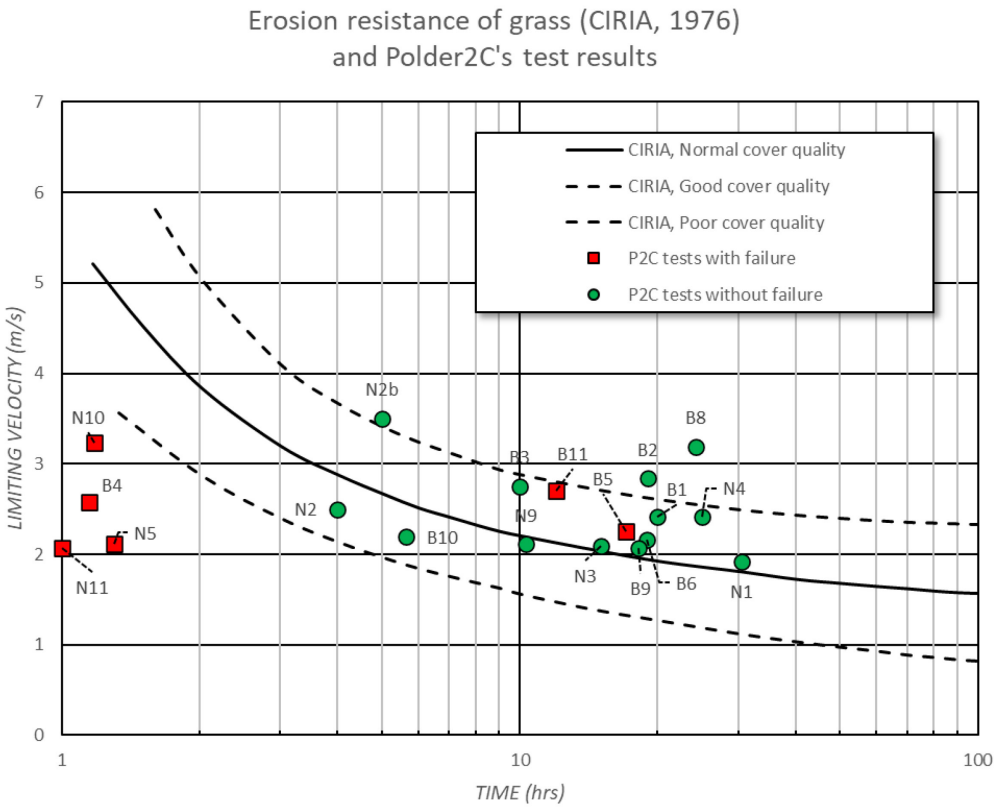

Figure 21 – Velocity, duration, and outcome of Polder2C's overflow tests compared to CIRIA (1976) erosion resistance of grass cover of different qualities. Velocities should be considered as low estimates (see text).

The cluster of tests with positive outcome, even after 30 hours, indicate that most of the levees, when in a normally maintained condition, are strong and can withstand an overflow event. Because the indicated velocities (measured at the upper slope) are a lower limit for the velocities further down the levee slope, the cover quality exceeds the "normal (and even good) cover quality", as indicated by the CIRIA curves, well. In other words, the tests indicate that the vegetated clay cover layer is even more resistant than what would be expected based on such curves. Thus, the tests that do not lead to failure indicate that most parts of the levee are in a normal to good condition because of the maintenance strategy applied.

In addition, tests that have been stopped without failure, also yield a lower limit for the time dimension on Figure 21, which means that all (Time, Limiting Velocity) couples for tests that did not lead to failure, can actually move upward and to the right on the graph, i.e. to a much more stable or favourable situation.

However, the levees protecting polders and other low-lying terrains is only as strong as its weakest part. In case of adversity, the 'good quality' parts will not be decisive for what happens, but the "poor quality parts" will. The cluster of early failures are related to the tests of slopes with anomalies: the reed fields on soft soil (tests N-OF10 and N-OF11) and the large animal burrow (N-OF05). Also, one test where smaller (mole) burrows (B-OF04) gave rise to sand outflow through the cover layer, failed quickly. Such anomalies are relatively easy to identify visually. Especially after mowing (as part of the normal maintenance), larger burrows and other vegetation or soil anomalies may be easily recognized. It is deemed feasible to include the

This project has received funding from the Interreg 2 Seas programme 2014-2020 co-funded by the European Regional Development Fund under subsidy contract No [2S07-023]

identification of such anomalies during regular levee inspection, and it would be advisable to mitigate or repair such anomalies as soon as possible after discovery. However, if unmanaged, such anomalies clearly prove to lead to failure within the duration of an overflow event in case of a tidal environment, and well within the duration of upstream (fluviatile) floods which may have durations of days. Several other short tests (N-OF5B, N-OF05C, N-OF06, N-OF07, N-OF08) are not shown in the graph because they relate to levee slopes without or poorly developed vegetation. The outcome of these experiments is that reinforced turf mats, geotextiles and other emergency repair solutions are insufficiently strong on the short term because regrowth of vegetation is lacking. Therefore, these do not relate to the erosion resistance of grass covers and are thus not included in the plot.

The two tests that failed after more than 10 hours of overflow can be interpreted in various ways. The goal of these were different: one was related to a slope morphology anomaly (B-OF05), which was shown afterwards involving a mole burrow through and under the clay cover. The other test (B-OF11) was organized to visualize the impact of a tree but ended up being influenced by smaller burrows as well. Despite the differences, the common – and probably decisive – factor for failure was the presence of burrows (a mechanism that may explain the time needed to failure to develop is explained in §4.2). This adds uncertainty in how fast the presence of burrows may lead to failure. The most conservative approach here – which is probably most suitable in a flood-protective function context – is that of early failure (as described above). A much less conservative approach is based on the fact that the reported velocities are measured on the upper slope, thus not fully developed to maximum velocity. With this, it can be argued that the vegetated cover was holding its strength as indicated by the CIRIA curves and that the failure still occurred at a time well beyond what would be expected from the lower CIRIA curve (for low quality covers).

The thickness of the clay cover is significantly lower in Belgium than in the Netherlands: +/- 0.30 m vs +/- 0.90 m. The 'unexpected' failures after about 10 hours both occurred on a Belgian levee, which is an indication that the thinner clay cover layer is much more vulnerable than a thicker clay cover layer. It can be expected indeed that if sand expulsion occurs under a thin clay layer, that this will be faster under critical stress than when a thick clay layer is undermined. Also, the travel path for the water through the clayer and thus the sand expulsion distance is also considerably smaller.

Nonetheless these different approaches to these failures, the fact that failure occurred within a cloud of non-failure tests, adds uncertainty to how reliable the cover quality is. The role and impact of burrows is discussed further in the text.

4.2 Evolution of the cover layer state for the reference cases

During an overflow test, the quality of the vegetation cover evolves through time. It was observed that this evolution was nearly identical in all reference tests. An overview of this evolution is shown in this paragraph by means of a series of pictures.

4.2.1 B-OF01 (Belgian Reference, 180L/s/m)

The initial condition of the grass cover shown (Figure 22 and Figure 23, '0 hours'), is after a brief moment of overflow with flattened grass and loose debris washed away. The state of the grass cover layer can be described as lumps of dense grass sods, interspaced by barren patches. Through the course of time, it is observed how the barren patches become more outspoken and more clearly visible, indicating that some grasses are being cut or eroded from the soil by

This project has received funding from the Interreg 2 Seas programme 2014-2020 co-funded by the European Regional Development Fund under subsidy contract No [2S07-023]

the current (Figure 22 and Figure 23, '2', '5' and '15 hours'). Consequently, the soil underneath is more exposed to the current. This process is occurring the entire levee slope but seems (qualitatively) be more outspoken on the lower part of the levee slope with higher current velocities.

Generally, there are no clear indications of strong erosion of the top layer. The cohesion of the cover layer appears to be high enough ensuring the integrity of the cover layer, with vegetation root systems, is strong enough to withstand long duration of continuous overflow.

4.2.2 N-OF01 (Dutch Reference, 180 L/s/m)

Figure 24 and Figure 25 show the initial condition ('0 hours') of the grass cover layer after a moment of overflow with the grass 'flattened' and loose debris washed away. The state of the grass cover layer can be described as a continuous grass cover with little barren space. Through the course of time (other timesteps), it is observed how a small number of limited barren area is becoming visible. The evolution is very slow and even after 15 hours barely visible at the upper part of the levee slope. At the lower part of the levee slope towards the transition to the toe of the levee, some pools are formed with standing water. These pools are not really evolving during the test, indicating the consistency of the grass cover layer is being kept very well.

4.2.3 B-OF09 (High discharge, 375 L/s/m)

Figure 26 shows the condition after 1 hour of overflow of the grass cover layer. The grass at this site is clearly longer than in the two previous tests, but still some barren patches are visible at the start of the experiment. After 15 hours of overflow, several new barren patches have evolved, and existing ones have grown. The evolution appears to be stronger (more removal of vegetation) than in two previous tests, because the load of the overflowing water on the vegetation and soil is expected to be stronger as well.

4.2.4 Comparison

For the reference grass cover layer, a strong contrast is noticed in onset and evolution of the cover layer state for the Dutch and the Belgian levee. The grass cover layer of the Dutch levee is continuous and effectively forming a cover, while the cover layer for the Belgian levee is patchy, discontinuous and shows barren spaces from the onset. This indicates that the surface of the landward slope of the Belgian levee is more uneven, probably caused by the intermittent presence of grazing sheep on the levee slopes. The practice of grazing on levees also occurs in the Netherlands, but not on this specific part of the levee**. The patchiness clearly show that the sheep cause small-scale damage to the surface and its vegetation cover, making it more prone to evolution of barren patches and erosion.** However, as the continuous overflow tests also indicate, **the irregularities do not compromise the integrity and erosion resistance as a whole (in contrast to larger anomalies described further in this report). Higher discharges appear to have negative impact as well.**

This project has received funding from the Interreg 2 Seas programme 2014-2020 co-funded by the European Regional Development Fund under subsidy contract No [2S07-023]

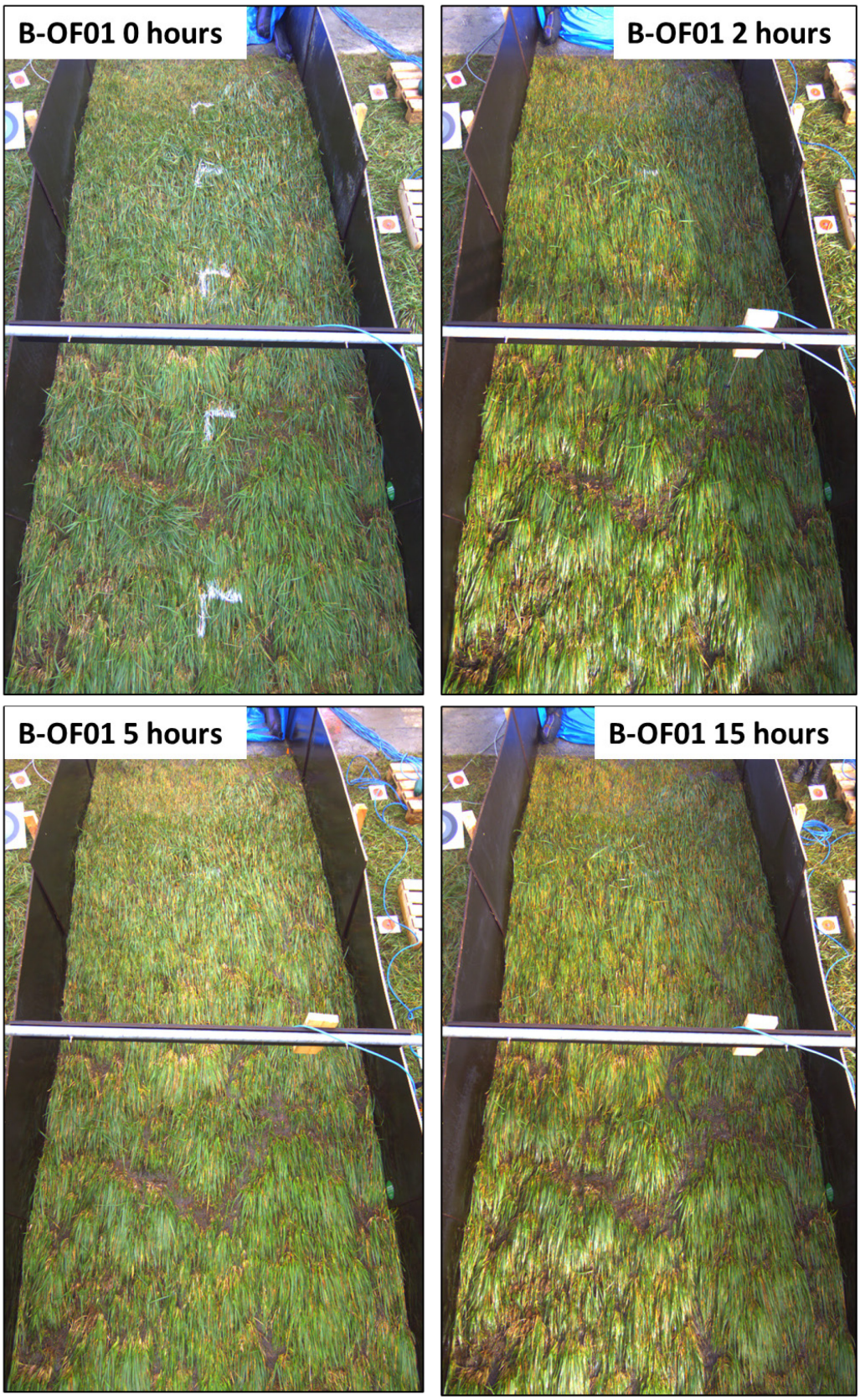

Figure 22 - Evolution of grass cover layer quality at B-OF01 site, upper slope, at different times during the experiment.

This project has received funding from the Interreg 2 Seas programme 2014-2020 co-funded by the European Regional Development Fund under subsidy contract No [2S07-023]

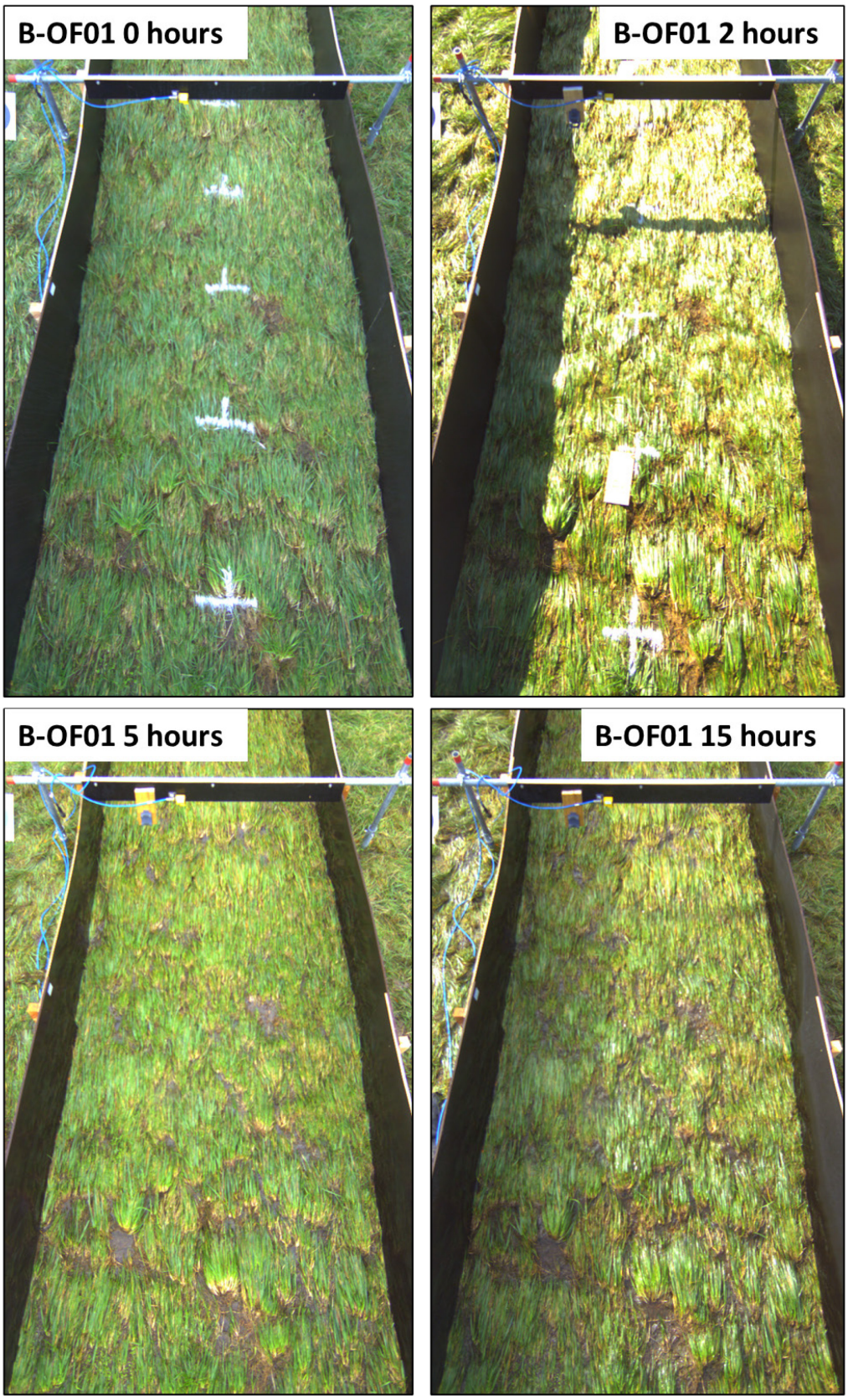

Figure 23 - Evolution of grass cover layer quality at B-OF01 site, lower slope, at different times during the experiment.

This project has received funding from the Interreg 2 Seas programme 2014-2020 co-funded by the European Regional Development Fund under subsidy contract No [2S07-023]

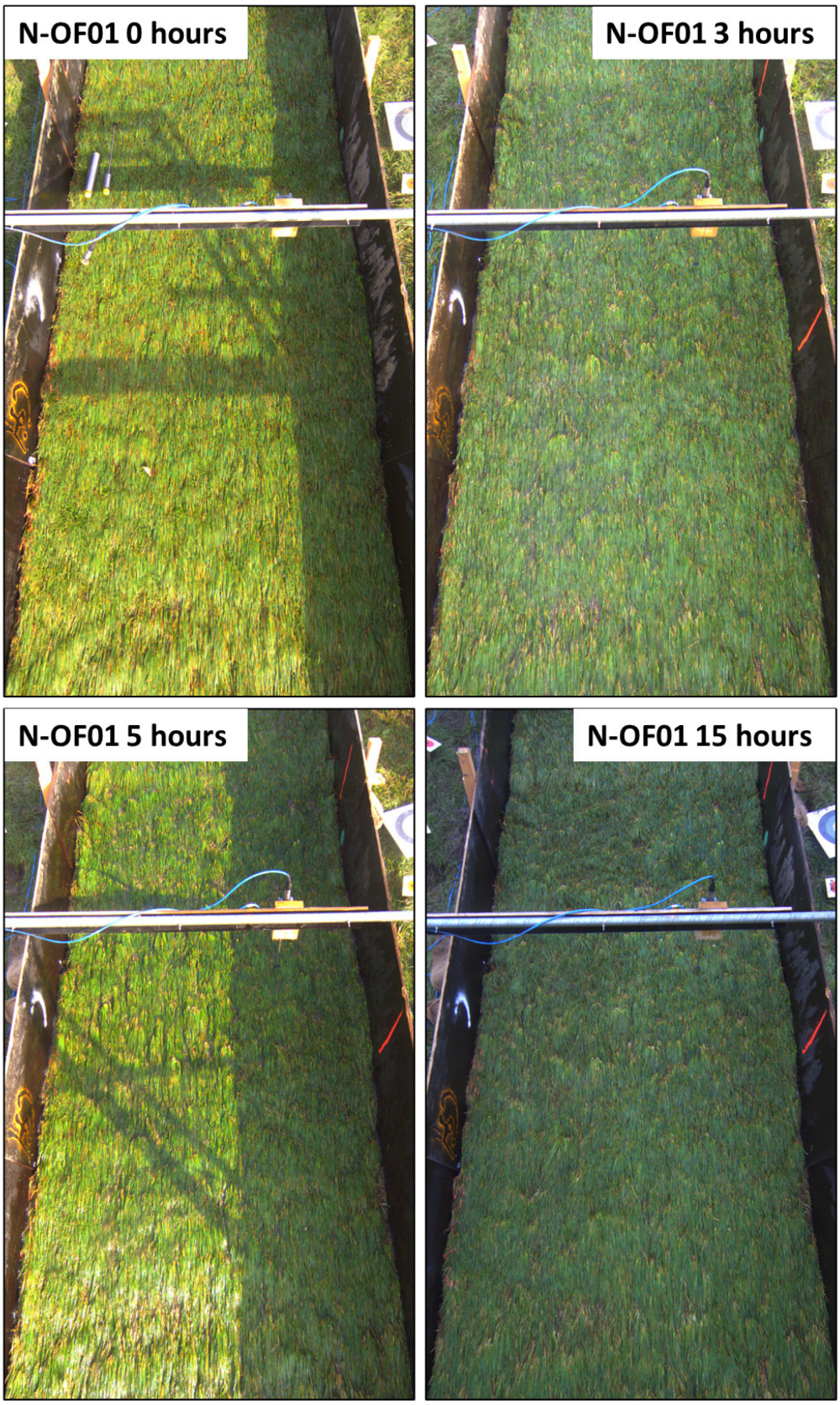

Figure 24 - Evolution of grass cover layer quality at N-OF01 site, upper slope, at different times during the experiment.

This project has received funding from the Interreg 2 Seas programme 2014-2020 co-funded by the European Regional Development Fund under subsidy contract No [2S07-023]

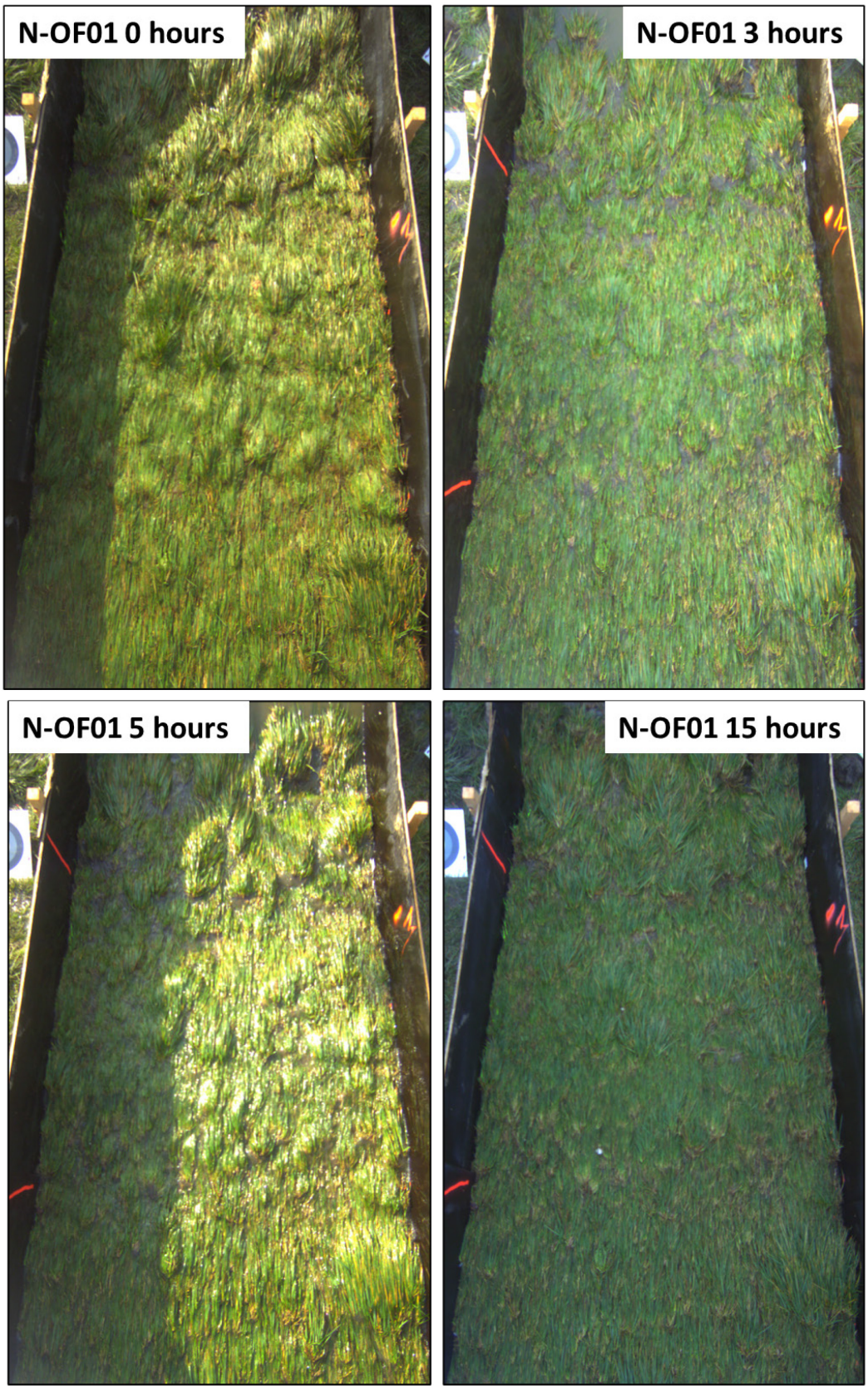

Figure 25 - Evolution of grass cover layer quality at N-OF01 site, lower slope, at different times during the experiment. Toe is towards the upper part of the image.

This project has received funding from the Interreg 2 Seas programme 2014-2020 co-funded by the European Regional Development Fund under subsidy contract No [2S07-023]

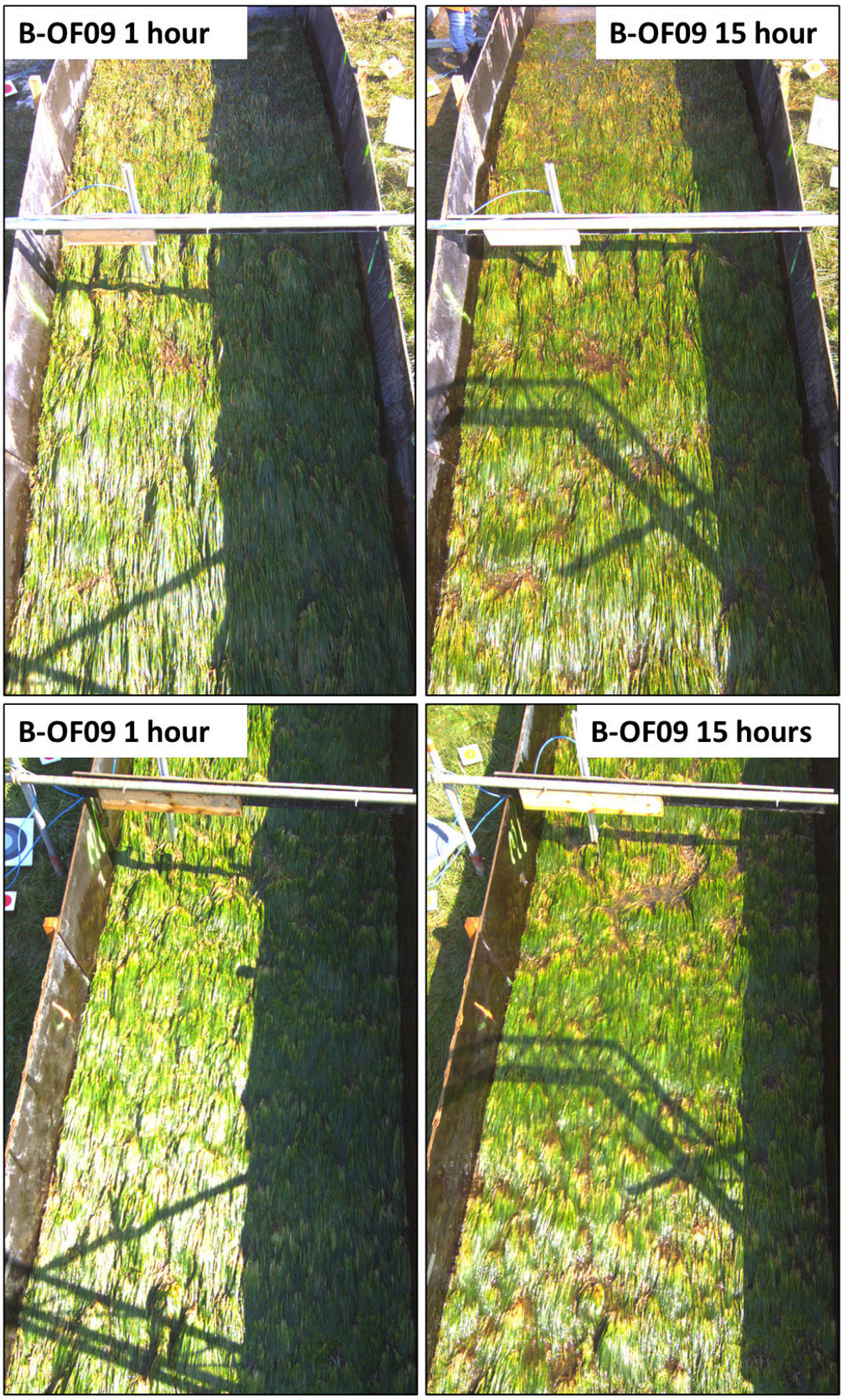

Figure 26 - Evolution of grass cover quality at B-OF09 site, upper (top row) and lower slope, at different times during the experiment.

This project has received funding from the Interreg 2 Seas programme 2014-2020 co-funded by the European Regional Development Fund under subsidy contract No [2S07-023]

4.3 Effect of animal burrows

Two test sections were specifically selected for the investigation of the effect of a large burrow (N-OF05) and protection of many small burrows visible on the surface (N-OF09) against erosion (see Tsimopolou & Koelewijn, 2022 for more information). During the experiments, other test sections seemed to have the presence of burrow systems (B-OF04, B-OF11, both in combination with a tree at the levee slope, and possible B-OF05). This influence of animal burrows led to the formulation of an internal erosion process hypothesis (see below). During some of the subsequent tests, artificial burrows were created in different sections (N-OF03, B-OF09 and B-OF11), typically towards the end of a test, to test whether the given process could be provoked.

4.3.1 Large burrow

The presence of a large burrow on the levee slope (Figure 27), as observed in test section N-OF05 was expected to be a critical feature that would undermine the slope during overflow. During the first minutes of the experiment, it was observed that the sand mound in front of the burrow was washed away, leading to very water with high turbidity for several minutes. After that, it was observed how a wire fence was exposed, signalling a prior repair action of this burrow. This prior repair was later confirmed by field inspectors of Waterschap Scheldestromen. During the overflow test, it was observed that erosion started to form a depression upwards of the wire fence protection (Figure 27). After 1 hour and 13 minutes of continuous overflow, a sudden collapse of the cover layer occurred inducing large amounts of sand and mud being washed away during a brief time. Consequently, the discharge pumps were shut down quickly and during the subsequent minutes, a retrograde collapse of the top layer was observed, resulting into a large damage with exposure of the internal sand core (Figure 28).

The continuous overflow test with the presence of a large animal burrow showed that such a feature forms a weak spot in the levee protection system leading to critical damage within just more than one hour. It was even suspected that the wire fence was stabilizing the depression above the animal burrow and that it thus was lengthening the damage evolution process.

Figure 27 – N-OF05: (left) initial burrow state and (right) exposure of wire fence (lower part of the image) and erosion depression (upper part of the image) during the experiment.

This project has received funding from the Interreg 2 Seas programme 2014-2020 co-funded by the European Regional Development Fund under subsidy contract No [2S07-023]

Figure 28 - N-OF05: Evolution of the damage during the last 15 minutes of the test; upper camera portal (= upper slope view).

4.3.2 Unexpected and artificial burrows

Less obvious burrow presence resulted in significant slope damage comparable to the one described in §4.3.1. The experiments in B-OF04, B-OF05 and B-OF11 were all conducted to investigate a tree at the levee toe or a morphological anomaly in the slope profile. Each of these three tests was related to a wider area with trees where sheep, occasionally present for grazing the levee slopes, had their resting place. The presence of the sheep had created damage to the levee slope (target of section B-OF05). Prior to these tests, there had been no specific attention to the presence of small (e.g., mice) burrows.

As described in Depreiter et al. (2023a), at the test section B-OF04 shortly after the onset of the test a significant outflow of water and sand was noticed from a burrow outside of the test section. After one hour and nine minutes of continuous overflow, the sand outflow resulted into a collapse of the cover layer.

At the test section B-OF11 (also see Tsimopoulou et al., 2022), burrows were also discovered within the test section. In order to provoke inflow of water into the sand core of the levee 'artificial' burrows (drillhole) were introduced towards the end of the experiment. These artificial burrows were created using a drillhole, interconnecting the ones inside with the ones outside the test section. This artificial animal burrow ultimately led to outflow of sand inside the test section at the toe of the levee where another animal burrow was detected (Figure 29).

This project has received funding from the Interreg 2 Seas programme 2014-2020 co-funded by the European Regional Development Fund under subsidy contract No [2S07-023]

The 'artificial' burrow outside the test section produced water outflow without significant amounts of sediment. Therefore, it was presumed the artificial burrow may have accelerated, but not caused an already ongoing process.

At the test section B-OF05 no large burrows were detected prior to the overflow test. Small burrows were at the start of the test not yet in scope and thus not discovered. However, after a long time of overflow (17 hours) with a specific discharge of 160 l/s/m, a large slope failure occurred. After damage repair, subsequent investigation uncovered a large mole burrow system within the test section, starting near the levee crest and involving downwards at the clay-sand interface. It had been shown that inflow of water into the sand core of the levee was effectively occurring (Hölscher et al., 2021).

Figure 29 - Sand outflow and boils outside the test section (left: B-OF04 outside the section; right: B-OF11 inside the section).

Figure 30 - Outcome of the B-OF04 (left) and B-OF11 test.

Figure 31 - B-OF05 site prior and after the overflow experiment.

This project has received funding from the Interreg 2 Seas programme 2014-2020 co-funded by the European Regional Development Fund under subsidy contract No [2S07-023]

Internal erosion process hypothesis

After the first unforeseen damage evolution due to animal burrows, an internal erosion process hypothesis was formulated as follows. This description is supported by images shown in the main text.

a) During the overflow experiments, the overflowing **water enters the cover layer of the levee** and the shallow sand core through cracks, animal burrows and other discontinuities (Figure 12 1, 2).

b) **A network of cracks, pipes, burrows, ... form preferential flow pathways which will locally** change the internal hydraulic grade line/the saturation line within the levee (2, 3).

c) **When a hydraulic exit point is present** at a lower point along the levee slope, the water will flow out (3) and depending on the flow velocity and the sediment properties, **sediment entrainment may occur**. Sediment entrainment with significant sediment volumes, leads to a mass deficit along the channel network (4).

d) **When also entrainment of sand from the levee core is present, the mass deficit will develop** below the cover layer which will remain intact thanks to its (tensile) strength of the grass cover layer on clay. If this mass deficit becomes large enough, an **initial depression** will develop (5), and will ultimately lead to **collapse of the cover layer, the** grass cover layer being tore apart and being collapsed into the mass deficit hole) (6). This latter collapse was observed during the field test.

e) Once the collapse has taken place, the hydraulic head established in the levee core needs to equilibrate, leading to outflow entraining large portions of sand from upstream (7). This leads to retrograde erosion and subsequent collapse of the levee cover layer (8) until the cliff stabilizes under the influence of desaturation.

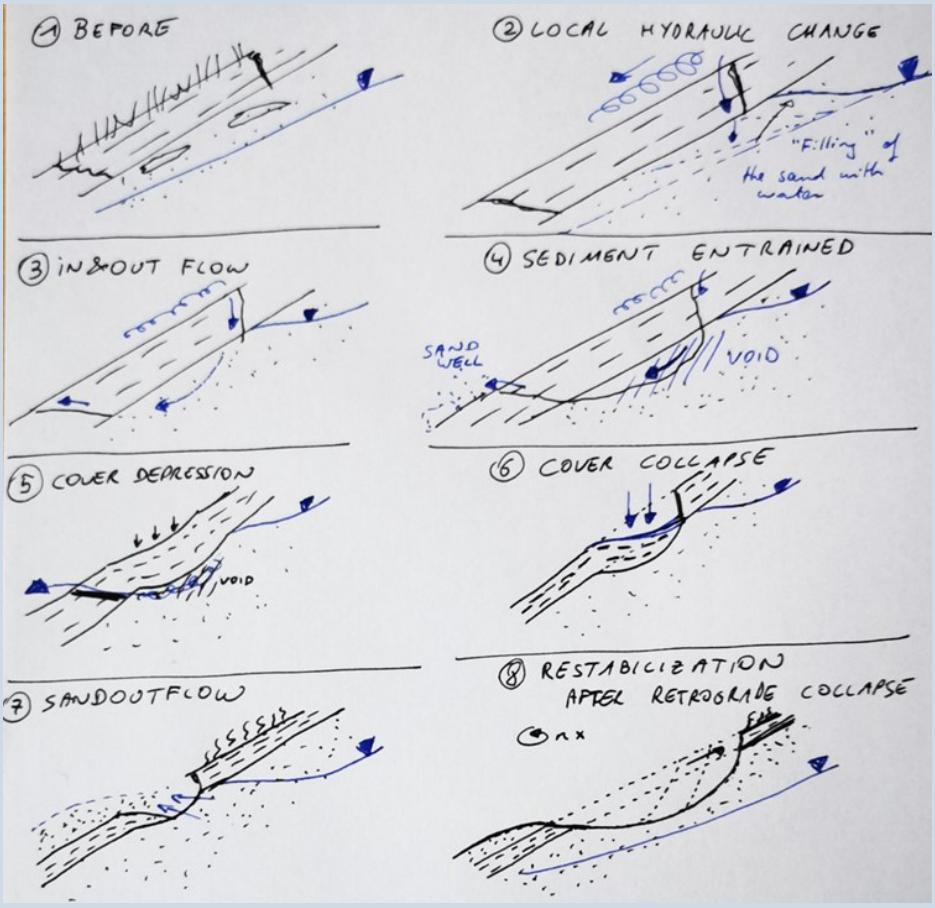

Figure 32 - Field sketch of the burrow induced failure process hypothesis.

This project has received funding from the Interreg 2 Seas programme 2014-2020 co-funded by the European Regional Development Fund under subsidy contract No [2S07-023]

The observations during the test at test stretch B-OF04 and B-OF05 led to the formulation of an initial erosion process hypothesis, which is described on the previous page. The 'artificial burrow' drillhole introduced during the test at test stretch B-OF11 was created based on this process, trying to provoke or accelerate the process.

On the Dutch part of the Hedwige-Prosperpolder levee, small burrows were also discovered and investigated. Tsimopoulou et al. (2022) present an extensive overview of animal burrows at different locations. Mapping and surveying of burrows systems, and testing connectivity with smoke and other methods was executed. Burrow systems were also grouted and excavated.

During the overflow test at test stretch N-OF03, 'artificial burrows' were also drilled. These burrows did not lead to any significant changes around the boreholes during the test. Natural burrows were discovered at the test stretch N-OF04, and were identified as mice burrows, but the presence of these burrows during this test did not lead to analogue observations as made during the tests on the Belgian test sections. The striking difference between the tests at test stretches N-OF-03 and N-OF-04 with the tests on the Belgian part of the levee is that the outflow of sand was not observed.

One of the variables influencing the mobilization of levee core sands via small burrows is the thickness of the clay cover layer. The thickness of the clay cover layer of the Belgian levees in this area is 30 to 50 cm whereas their Dutch counterparts have clay lavers of 80 to 100 cm (Figure 33). This difference may be enough to prevent small burrows either entering the sand core or leading to sand expulsion at the surface.

4.3.3 Illustrations of the burrow induced failure process hypothesis

Inflow of water into the levee core (step 2-3 in the process hypothesis)

On several occasions, water flowing out of the levee through burrow systems was observed, meaning there also must be an influx. The 'artificial' burrow drillholes showed not to be effective to provoke the slope failure process. Different factors may play a role: the drillholes were closely positioned limiting the distance between entrance and exit points; if a connection between two holes was present, the length of the entire 'burrow' was very limited and even close to zero, as during test B-OF11. Another setup with a bigger distance between the drillholes, as in N-OF03, did not create an effective connected 'burrow', which would also prevent through-flow. Consequently, it the 'sand entrainment length' of the burrow is defined as the distance over which water is flowing and effectively capable of removing sand further assisted by the roughness of the burrow itself, a natural burrow would have a much greater sand entrainment length than either form of artificial burrows that were produced.

To conclude, the steps 2 and 3, the in- and outflow and saturating a part of the sand core with water, in the process hypothesis seem to be related to the presence of burrows along which water can infiltrate in the cover layer and flow through.

Sand entrainment and cover depression (step 4-5)

The sand entrainment and expulsion near the levee toe has been observed on several occasions. After sand has been entrained from underneath the cover layer, the support of the cover layer is missing. Step 5 in the process hypothesis has effectively been observed and documented for the test B-OF11. During this test where a depression of the cover layer was clearly present, indicating the presence of a void below the cover layer, which is cohesive and

This project has received funding from the Interreg 2 Seas programme 2014-2020 co-funded by the European Regional Development Fund under subsidy contract No [2S07-023]

held together by the root system of the vegetation layer. It is reasonable to expect that a thinner cover layer will be more susceptible to this process than a thicker cover layer.

Figure 33 - Internal structure of the levee near N-OF05 during excavation. The clay cover layer is less approx. 80 to 100 cm thick.

Collapse and outflow (step 6-7)

The outflow of liquified sand and especially the further (retrograde) collapse of the cover layer is well documented in test B-OF04 and in test B-OF11. This is shown in Figure 14 to Figure 16. During these experiments, the overflow discharge was evidently stopped as soon as such failure occurred in order to prevent damage that would not be easily managed afterwards. In real overflow conditions, this would evidently not be the case, and may lead to further erosion and ultimately to breach formation. After the shutdown of the overflow generator, a collapse of the cover layer iterating a number of times is observed as sand flows away from underneath the upslope cover layer. Regression was observed up to 2 meters upstream of the original collapse location.

Restabilization

The dewatering of the sand core filled with water, occurs simultaneously with the collapse process and it is expected that the process is stopped when the sand regains strength. If the overflow stops the erosive force of the water is taken away and the sand core and cover layer restabilize, yielding a state as observed in the experiments.

This project has received funding from the Interreg 2 Seas programme 2014-2020 co-funded by the European Regional Development Fund under subsidy contract No [2S07-023]

Figure 34 - Depression of the cover layer before the last run (left) and the collapse and erosion afterwards (right) during test B-OF11 (Photos: A. Koelewijn).

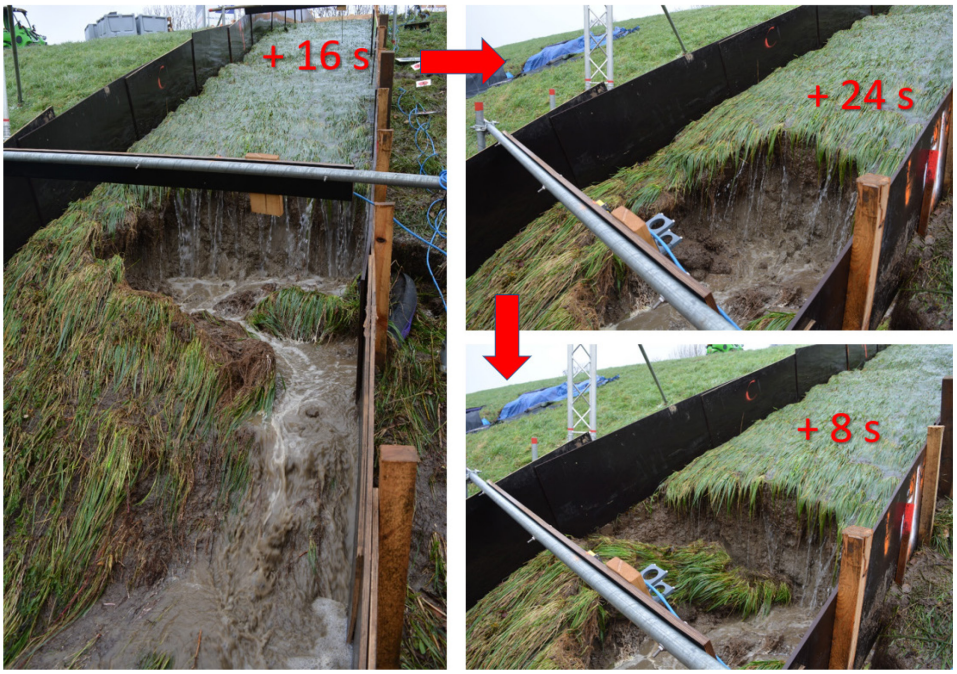

Figure 35 - Collapse and heads scarp regression during test B-OF04. (Photos: A. Koelewijn)

This project has received funding from the Interreg 2 Seas programme 2014-2020 co-funded by the European Regional Development Fund under subsidy contract No [2S07-023]

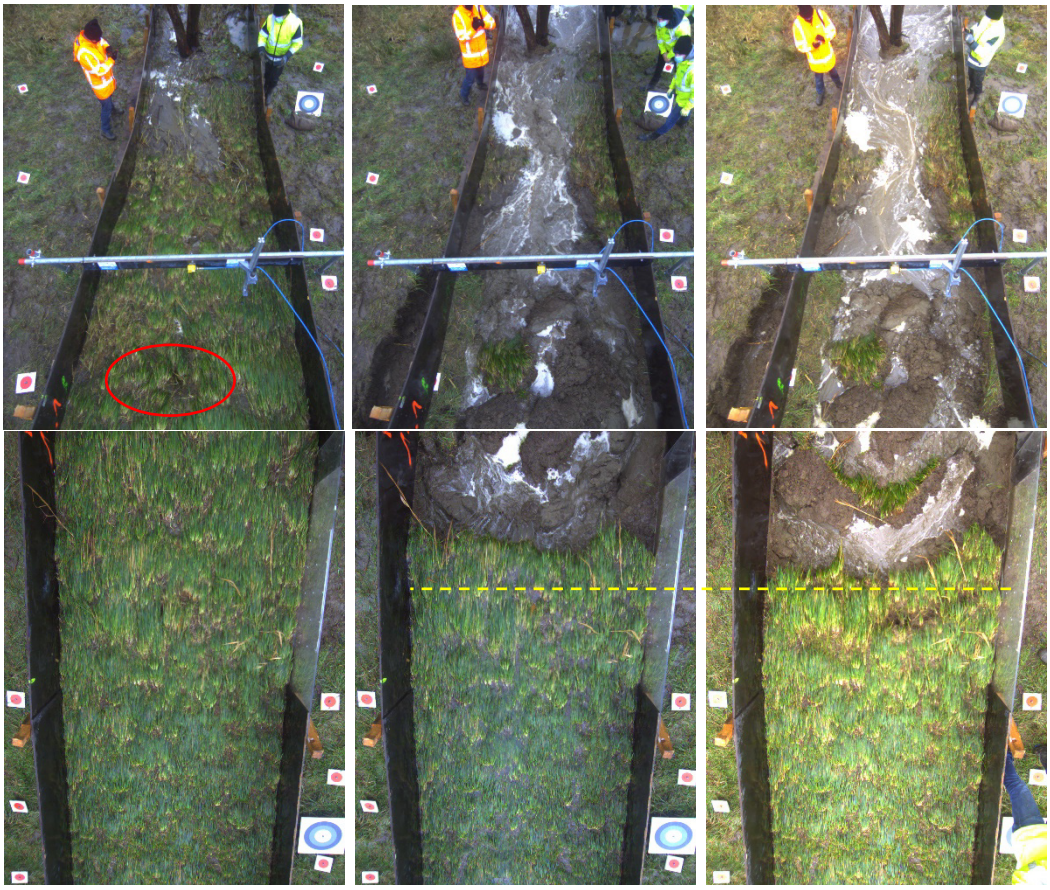

Figure 36 - Sequence of photos during the failure at test B-OF11. Left: 14:54 before the last overtopping activity. The initial depression is indicated by a red circle; Middle: 14:59, flow already stopped, and collapse has occurred; Right: 15:04, further collapse of the head scarp is ongoing. Yellow striped line indicates progression. Note that further tearing of the top layer is occurring beyond this line.

The observations related to the burrows lead to the following conclusions:

- the presence of cover layer piercing burrows (large burrows, e.g., rabbit and mole; or even smaller burrows, e.g., by mice) are expected to provoke sediment entrainment from underneath the clay cover layer during an overflow event.
- the sand expulsion from inside the levee can lead to an unsupported cover layer within the timeframe of tens of minutes to a few hours, i.e., within the time range of a real overflow event.
- the process leads to collapse of the cover layer and leads to large-scale slope failure which is further sustained by the presence of liquified sands of the sand core.
- following the fluid expulsion combined with retrograde head scarp erosion or collapse, the situation stabilizes when stopping the continuous overflow. However, in real-life overflow situations, where overflow is not stopped at the onset of the collapse, the consequences are expected to be even more significant due to ongoing erosion and potentially full breaching of the levee.

The presence of small burrows may not immediately lead to failure, but when given time, or recurrence of overflow, a failure process may be triggered. The tests prove that levee inspection, maintenance and mitigation or repair of anomalies are of paramount importance. Anomalies that are susceptible to erosion can very quickly develop into sand core exposure.

This project has received funding from the Interreg 2 Seas programme 2014-2020 co-funded by the European Regional Development Fund under subsidy contract No [2S07-023]

Given the fact that retrograde erosion evolves quickly and within minutes, such damage may evolve into full-blown breaches during a single overflow event. The magnitude and velocity of the damage evolution was surprising during the overflow tests and indicate that the design properties of levee systems can be undermined by seemingly unimportant features.

With these tests, weak links in the chain of protection was discovered, and careful evaluation will be needed on how mitigation, emergency measures and maintenance include this unknown in the levee management process.

4.4 Effect of alternative vegetation

4.4.1 Short vegetation

The **short(er) vegetation** (10 to 20 cm in length compared to typically 20 to 40 cm after 'regular' mowing[2]) in test B-OF02 did not result into faster erosion or damage of the levee slope, even though the shorter length could give less protection to the underlying soil. This does not seem to be the case. In terms of damage evolution, images of the cover layer (Figure 37, Figure 38) can be compared after a similar overflow time. For this purpose, the cover layer state after approximately 15 hours of overflow is considered:

- after 15:17 hours for the reference test B-OF01,
- after 15:01 hours for the test B-OF02 with the shorter grass.

Near the crest, it is observed that in between parts of vegetated slope, barren patches of clay are visible. The root systems of the grass are somewhat exposed. The image is very similar for both cases. On the lower half of the slope, both sections show larger pieces of barren soil. Here too, the general aspect is very similar despite the differences in vegetation length.

The hydraulic data also shows differences (Table 4), but given the overall spread on the data, no hard conclusions could be derived from this.

From this single experiment with short grass, it cannot be concluded that short grass negatively or positively influences the erosion or damage evolution compared to a reference vegetation on a Belgian levee.

Table 4 - Statistics for the reference test B-OF01 and the test B-OF02 with shorter grass.

Parameter	B-OF01 (Reference)	B-OF02 (Short grass)	B-OF02 – B-OF01
Discharge	356.0 L/s	333.0 L/s	- 23 L/s
Crest water height	18.3 cm	12.2 cm	- 6.1 cm
Upper slope height	7.3 cm	9.1 cm	+1.8 cm
Mid slope height	6.1 cm	7.9 cm	+1.8 cm
Lower slope height	10.3 cm	16.9 cm	+6.6 cm

[2] *During summer, vegetation height may be much higher than 40 cm, even over 1 m. Mowing is carried out several times during a growth season. The situation that is actual during the experiments is the state after the last mowing of the given season, and thus representative for fall and winter conditions, the period during which overflow is most likely to occur.*

This project has received funding from the Interreg 2 Seas programme 2014-2020 co-funded by the European Regional Development Fund under subsidy contract No [2S07-023]

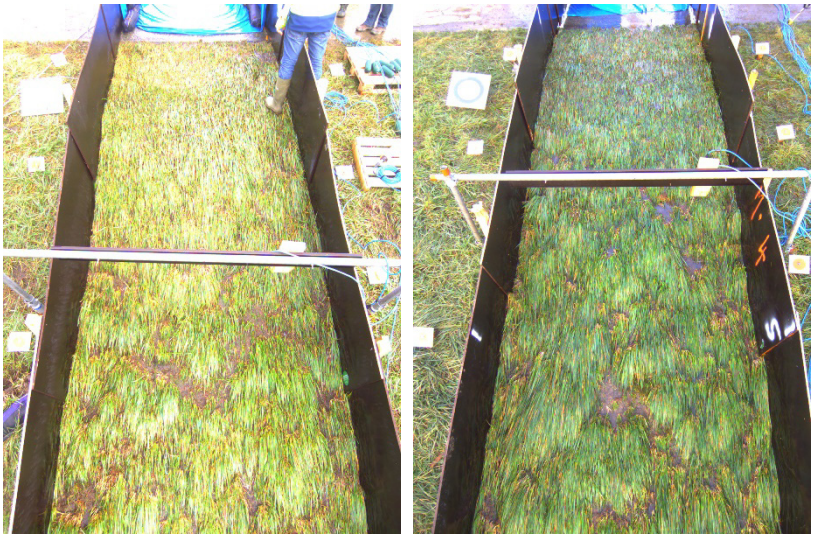

Figure 37: Visual comparison of B-OF01 and B-OF02 (upper slope) after 15 hours of overflow.

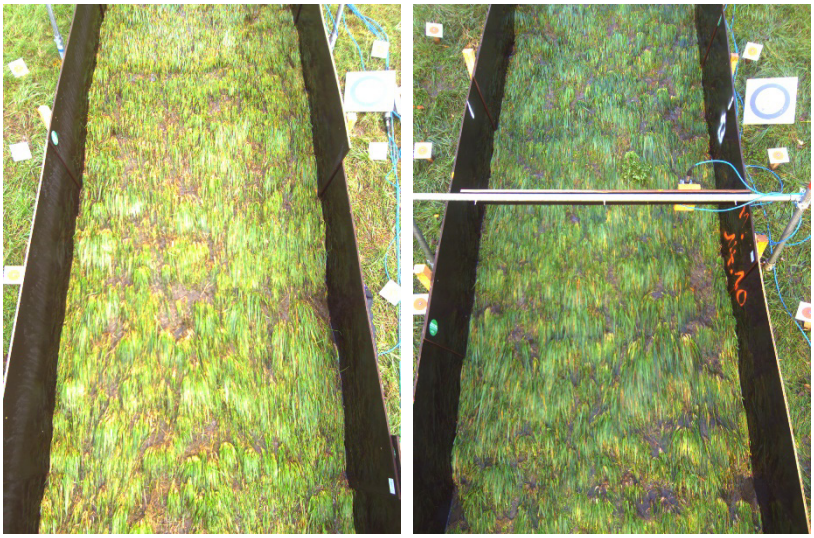

Figure 38: Visual comparison of B-OF01 and B-OF02 (lower slope) after 15 hours of overflow.

4.4.2 Reed patches on soft soil

On the Dutch part of the levee, a reed patch was present in an area with soft soil due to a limited drainage (a gravel draining is present at the toe of the levee). The reed patch had developed because no mowing was executed during several years. It was expected that either the dense root system of the reed field would stabilize the levee slope, or that the soft soil would quickly erode and lead to failure (see N-OF10, N-OF11 in Figure 21).

Two tests were organized on the reed filed: test N-OF10 and test N-OF11, see Depreiter et al., 2023b. The outcome of these tests was clear: within minutes, soil started to erode. The root system did stabilize part of the area, but other parts eroded quickly and deeply. During the first test the sand core started to destabilize after 1 hour of testing. During the adjacent test the destabilisation started after 31 minutes of continuous overflow.

This project has received funding from the Interreg 2 Seas programme 2014-2020 co-funded by the European Regional Development Fund under subsidy contract No [2S07-023]

Figure 39 - Two parallel test sections in the reed overgrowth.

Figure 40 - Detail of the damage on the upper side of the reed field after 30 minutes of overflow.

This project has received funding from the Interreg 2 Seas programme 2014-2020 co-funded by the European Regional Development Fund under subsidy contract No [2S07-023]

It may be concluded from these tests that soft soil and overgrown areas, such as the one observed, be it due to incipient piping, a clogged drain, or other processes, should be managed and repaired. Such areas represent a weak part of the levee and are vulnerable to levee destabilization during an overflow event.

4.4.3 Trees

Two experiments were executed to assess the impact of a tree at the toe of the levee: test B-OF04 and test B-OF11. The test B-OF04 was a very short experiment due to early slope failure and no observations related to the tree could be made (for detailed discussion, see §4.3.2). The test B-OF11 lasted longer (13 hours). During both experiments, the soil around the root system of the tree was eroding and gradually exposing the roots of the tree running shallowly (centimetres) underground. This process does not lead to very strong erosion around the tree trunk itself but is more widespread. Therefore, the erosion does not destabilize the tree, nor it compromise the strength or stability of the levee.

Figure 41 - Overflow with tree at the levee toe (B-OF11).

Therefore, no negative direct impact of the tree on the levee stability is observed. Within the timeframe of a real overflow event, the tree will likely not lead to a problematic situation.
It must be noted, however, that these tests were conducted under fair weather conditions, and that other processes such as treefall due to storm winds, cannot be evaluated based on these tests. It is also not clear whether the vulnerability of the tree itself has increased. This will probably depend on the root structure of the tree.
An indirect effect of a tree on a levee may be the fact that tree areas may serve as shelter and sleeping places for grazing animals on the levee, which was observed at this location. This is inducing other types of damages, like damage to the levee slope (as in test B-OF05); attraction of other animals (and their burrows), etc.

This project has received funding from the Interreg 2 Seas programme 2014-2020 co-funded by the European Regional Development Fund under subsidy contract No [2S07-023]

5 Insights from wave overtopping tests

In this chapter, a summary of insights yielded from the wave overtopping tests performed on (Dutch) levees in the Hedwige-Prosperpolder are given. An overview as well as detailed pictures before, during and after each wave set) can be found in Daamen et al. (2022).

Hereafter, insights directly derived from the findings in the field are described. In addition, test outcomes are compared to damage predictions by the cumulative overload method (§3.2.2 and van der Meer et al., 2010).

5.1 Overtopping test outcome

The strength of the existing levee cover was tested at four test sections in levee stretch VI. Various tests conditions were considered on each of these test sections, whereby the wave overtopping discharge (and thus the load) was incrementally increased during each test. Five different irregular wave overtopping conditions were tested, including one condition that included overflow as well (see Infram, 2022). The test conditions ranged from frequent small waves (e.g., equivalent discharge of 60 L/s/m and significant wave height of Hs=0.5 m) to less frequent, e.g., 100 L/s/m and Hs=2.0 m). The tests with the small waves are hereby representative for the Belgian and Dutch riverine levees while the tests with the big waves are more representative for the Dutch coastal levees. Each wave condition is applied for 2 "storm hours", which can take longer in duration due to a limited filling discharge of the device. Because the impact is more important than the duration (see further), this is not considered problematic for the test.

The following terms are used when describing the changes in a test section:

- "Rinse clean", i.e., a small overtopping set to wash away loose vegetation and debris.
- "Initiation of damage": i.e., visible barren spots, erosion, without integrity compromise.
- "Failure of the cover": the integrity of the cover layer fails, with potentially strongly evolving slope failure.

5.1.1 N-OT01

A well-maintained levee cover with a uniform vegetation and presence of some bare spots and molehills from the start, was able to withstand consecutively all 5 wave sets (Figure 42, a. to c.). Continuously repeating wave set V made the cover to fail after 3 storm hours.

5 consecutive wave sets did not result in failure. Mole holes rinsed out gradually with time and from the third wave set on, a gravel box at the toe, which serves as drain, became visible. Near the end of the third wave set, sand from the levee core was released from a mole hole outside the test section (Figure 43), allowing overtopping water to flow out). After the 4th set, a small region 15 m down the slope (box 15CD[3]) started to subside (initiation of damage), indicating undermining, presumably following erosion of the sandy core underneath via connecting mole holes. The 5th set of wavesworsened the decline of the entire levee slope. When continuing the experiments by repeating the 5th wave set, one meter upwards of this subsidence (box 14CD), the area suddenly failed after 3 storm hours. 45 minutes of storm later, an erosion pit of 3m by 4m and a depth up to 1m was formed due to the overtopping waves that dived into it.

[3] *The test section is divided in square boxes of 1m². Each is numbered as a distance from the top and indicated with a letter (A-D) from left to right (looking downward) accross the slope. Therefore, Box 15CD indicates a distance of 15 m down the slope, on the right hand side of the slope (looking downward).*

This project has received funding from the Interreg 2 Seas programme 2014-2020 co-funded by the European Regional Development Fund under subsidy contract No [2S07-023]

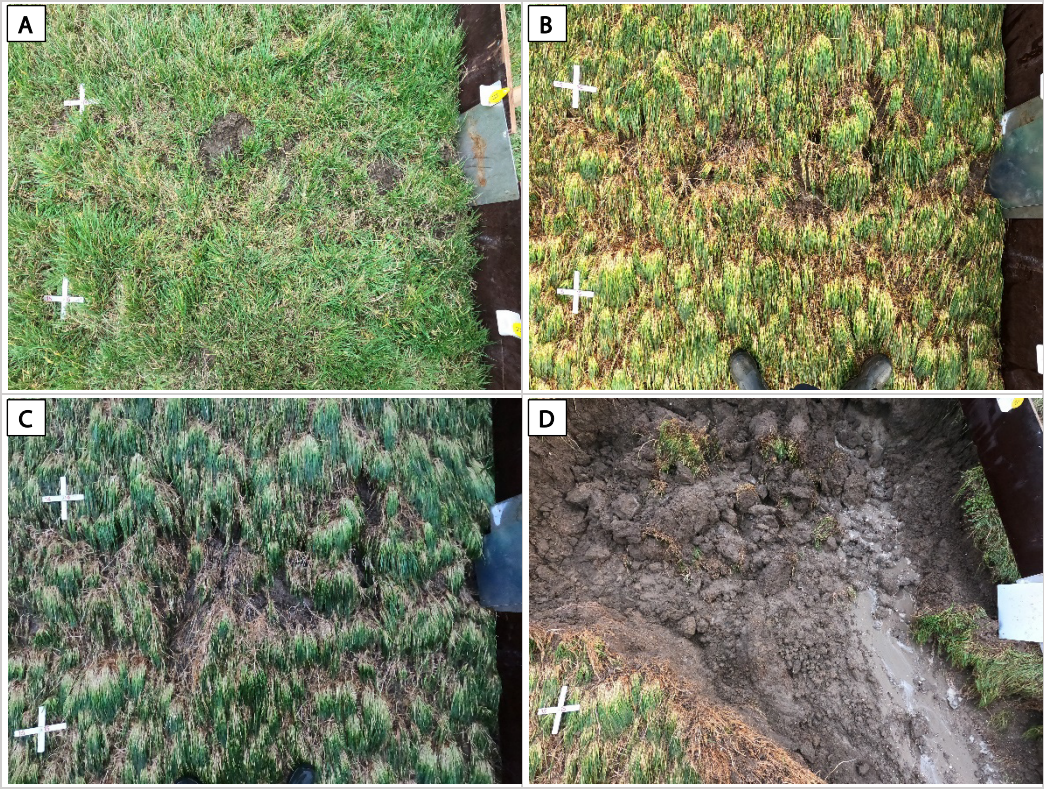

Figure 42 – Detail of levee slope of N-OT01 (box 13-14CD): A) at the start, B) after wave sets I, II, III and IV, C) after wave sets I, II, III, IV and V and D) continuing with wave set V for an extra 3 hours and 45 minutes of storm.

Figure 43 - Sand released through a mole hole outside the test section after 4 sets of waves.

This project has received funding from the Interreg 2 Seas programme 2014-2020 co-funded by the European Regional Development Fund under subsidy contract No [2S07-023]

5.1.2 N-OT02

A wet spot along the slope at boxes 17-20CD showed considerable erosion of the clay cover following wave overtopping. During the first set of waves, local bare spots became visible, which enlarged gradually (Figure 44, b.). The second set of waves led to removal of the vegetation over a larger area and yielded superficial erosion up to 15 cm (initiation of damage, Figure 44, c.). The 3rd set of waves yielded considerable erosion of ~25 cm (Figure 44, d). An erosion depth up to 35 cm (near failure) was noticed after the first storm hour of the 5th set, when the experiment was ceased (Figure 44, f.).

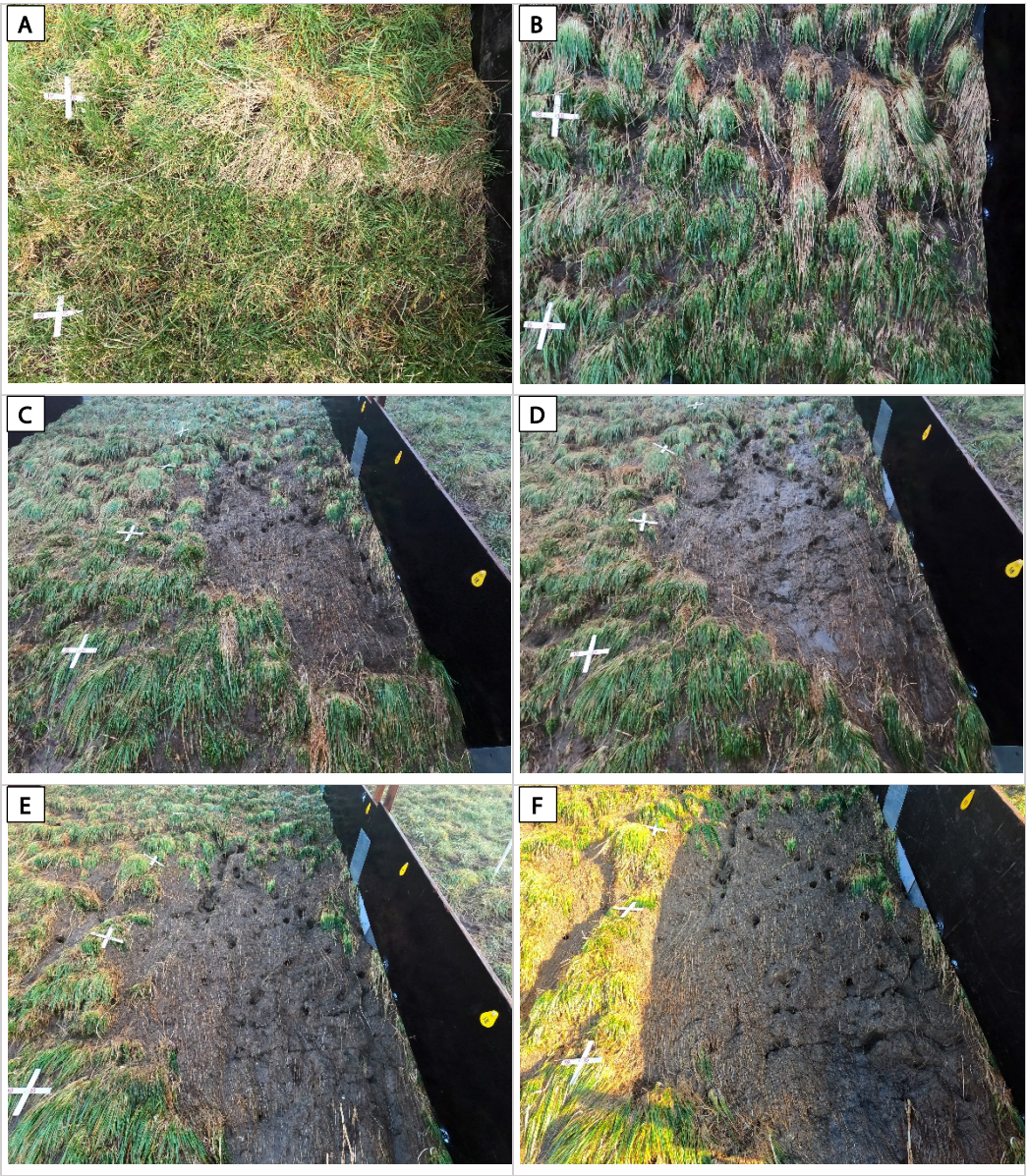

Figure 44 – Detail of levee slope of N-OT02 (box 18-19CD): – A) at the start, B) after wave set I, C) after wave sets I & II, D) after wave sets I, II & III, E) after wave sets I, II, III & IV and F) continuing with 1 storm hour of wave set V.

This project has received funding from the Interreg 2 Seas programme 2014-2020 co-funded by the European Regional Development Fund under subsidy contract No [2S07-023]

5.1.3 N-OT03

A slope with presence of a lot of animal burrows showed no serious damage. After the third set of waves, the gravel box at the toe became again visible. Bare spots grew and became more and more noticeable (Figure 45, b.). Continuing by repeating the third wave set for 1 storm hour yielded bigger bare spots but gave no signs of imminent failure of the cover (Figure 45, c.).

Therefore, 2 artificial burrows (ø = 10 cm) were drilled, in line with each other, one in the higher (boxes 8-9/9-10) and one in the lower (boxes 17-18/18-18) part of the slope, each consisting of an upward vertical pipe (angle of 90°) connecting with a downward more or less horizontally (angle of -10°) pipe and touching upon the sandy core (Figure 46). Eventually, the cover (with artificial burrows) did not fail (Figure 45, d.).

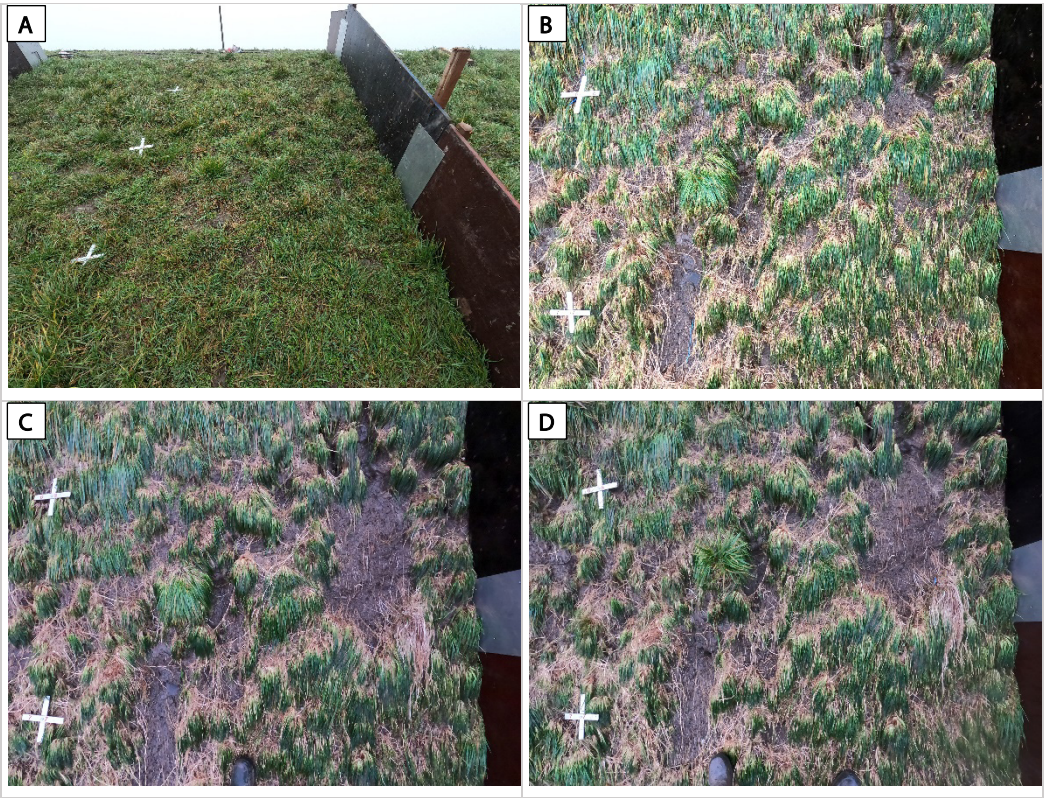

Figure 45 – Detail of levee slope of N-OT03 (box 6-7CD): A) at the start, B) after waves set I, II & III, C) after repeating III for 1 storm hour and D) after repeating III for 2 storm hours.

This project has received funding from the Interreg 2 Seas programme 2014-2020 co-funded by the European Regional Development Fund under subsidy contract No [2S07-023]

Figure 46 – Drilled burrows with in- and outlet in the centre line of boxes 8-9 and 9-10.

5.1.4 N-OT04

Another reference section was put to the test. When after 3 sets of waves no failure of the cover was imminent (Figure 47), 2 long(er) artificial burrows were created, adjacent in the higher part of the slope, again with a diameter 10 cm but by increasing the total length of the pipe (inlet of pipe at an angle of 45°, outlet of pipe at an anlge of -12,5°) (Figure 48). Both pipes were connected within the sandy core. Next, after applying wave set '2m50lsm' for 30 minutes both pipes showed washout of sand. Continuing with wave set III ('1m190lsm'), transport of sand remained and after 15', suddenly, a pit was formed at the inlet of 1 pipe (failure of the cover) (Figure 49). Gradually this pit eroded further and found connection to the other pipe inlet. 15' later, a step of 3m by 4m with a cliff of 1 m height was formed (Figure 50. Notice that both outlet pipes are still in place.

This project has received funding from the Interreg 2 Seas programme 2014-2020 co-funded by the European Regional Development Fund under subsidy contract No [2S07-023]

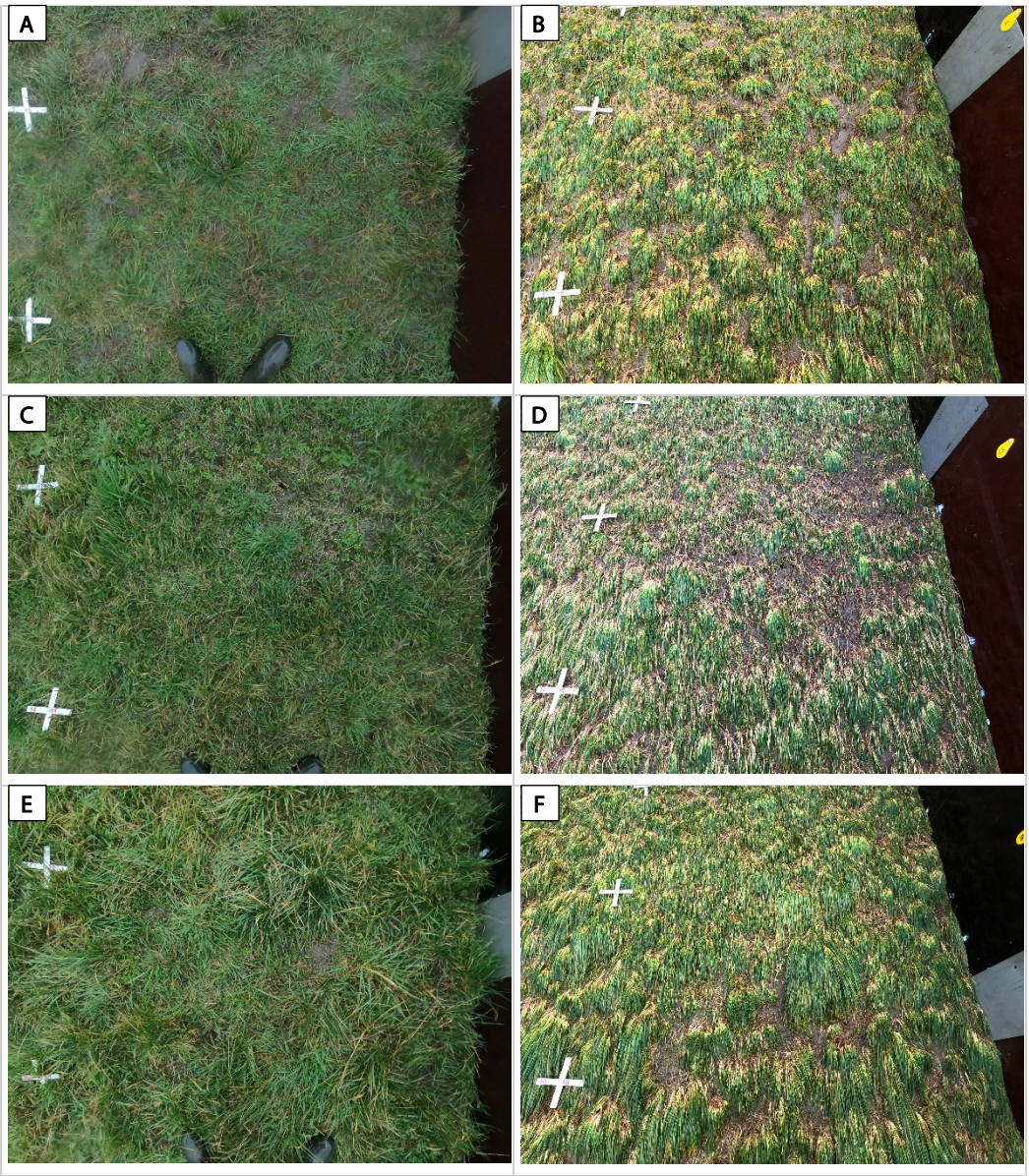

Figure 47 – Detail of levee slope of N-OT04 - box 5-6: A) at the start and B) after waves set I, III & III; box 13-14: C) at the start and D) after waves set I, III & III; box 18-19: E) at the start and F) after waves set I, III & III

This project has received funding from the Interreg 2 Seas programme 2014-2020 co-funded by the European Regional Development Fund under subsidy contract No [2S07-023]

Figure 48 – Drilling of 2 adjacent burrows during test N-OT04 with inlet in box 7-8AB/CD and outlet in box 13-14AB/CD

Figure 49 – Erosion pit around pipe inlet in box 7-8CD during the N-OT04 test (15' after start of wave set III)

Figure 50 – Large erosion pit around both pipe inlets in box 7-8AB/CD as outcome of the N-OT04 test (30' after start of wave set III)

This project has received funding from the Interreg 2 Seas programme 2014-2020 co-funded by the European Regional Development Fund under subsidy contract No [2S07-023]

5.2 Application of the cumulative overload method

The impact or the maximum flow velocity of the overtopping wave is more important than the duration of the flow (van der Meer et al., 2010). The "cumulative overload" function is an erosional index in which the overtopping duration is not considered, but sums the (square of the) velocity above a critical velocity, the overload above a certain threshold:

$$\sum(u^2 - u_c^2) \qquad (m^2/s^2)$$

With u_c the critical velocity, which is a strength parameter of the grass cover, and u, the front velocity of the overtopping wave.

As a guide to interpretation, van der Meer et al (2010) indicates the following table.

Table 5 – Cumulative overload treshold values (van der Meer et al., 2010)

Cumulative overload (m^2/s^2)	Interpretation
+ 500	Start of damage
+ 1000	Various damaged locations
+ 3500	Failure due to animal activity, surface irregularities
- 6000	Non-failure for well-maintained slopes

It is understood that u_c will typically be in the range of 4 to 7 m/s for well-maintained grass covers without open spots. The start of damage, and various damaged locations is hard to predict accurately, but in general, failure is estimated rather well.

The wave front velocities along the levee slope are shown in Figure 20 (see §3.2.2). The velocities are situated between 3.5 and 8.5 m/s, but most of the velocities recorded are between 4 and 6 m/s, with the higher values only occurring for the largest waves.

For each test section, provided the set of waves, the cumulative overload method can be used to estimate the moment of initial damage and/or failure of the vegetation cover, given the critical flow rate of the grass sod. Therefore, grass sod pull tests were executed to obtain the critical normal stress from which the critical flow velocities can be derived (Table 6). Due to an unsaturated cover layer, the outcomes in Table 6 are most likely overestimates. A noticeable difference in critical velocity for both levee stretches was found.

Note that the overtopping tests herein reported are all executed in levee section VI, thus a critical velocity of 5.0 m/s can be applied. Based on the wave front velocities, it is seen that larger waves exceed the velocity of 5 m/s and thus that damage may develop during prolonged wave overtopping.

Table 6 - Critical flow velocities following grass sod pull tests

Levee stretch	u_c (m/s)
IV	~6,5
VI	~5,0

This project has received funding from the Interreg 2 Seas programme 2014-2020 co-funded by the European Regional Development Fund under subsidy contract No [2S07-023]

5.2.1 N-OT01

The wave condition sets (indicated with Roman numerals) applied on levee stretch N-OT01 are 0.5m60l/s/m (I), 0.5m60l/s/m+ov (II), 1m190l/s/m (III), 2m50l/s/m (IV) and 2m100l/s/m (V); the last condition was repeated to simulate 3 storm hours instead of 2 storm hours. On the images in this section, the vertical lines indicate transitions in wave condition sets.

The predicted result for different critical velocities is indicated in Figure 51. The curve for u_c = 5 m/s is applicable here. Figure 51 indicates that during the third condition, initial damage would be appearing and evolve into failure during the most intensive wave set at the end of the test.

Initial damage was already present at the end of condition I (0.5m60lsm) due to the presence of (a small number of) mole burrows. This is more severe than expected on the basis of the model (the red curve in Figure 51). A buried gravel drain situated at the toe became visible towards the end of condition II (0.5m60lsmov) and was further exposed during condition III (1m190lsm). This did not impact the levee slope itself. During condition III (1m190lsm), expulsion of sand through the mole burrows, adjacent to the test section, became apparent and led to a surface depression due to undermining of the cover layer during condition IV (2m50lsm). Condition V (2m100lsm) was prolonged (repeated) and after further sand expulsion, the levee slope collapsed towards at the end of the test. Subsequent wave impacts further eroded the damage. The outcome of the test thus seems in line with the expected slope behaviour.

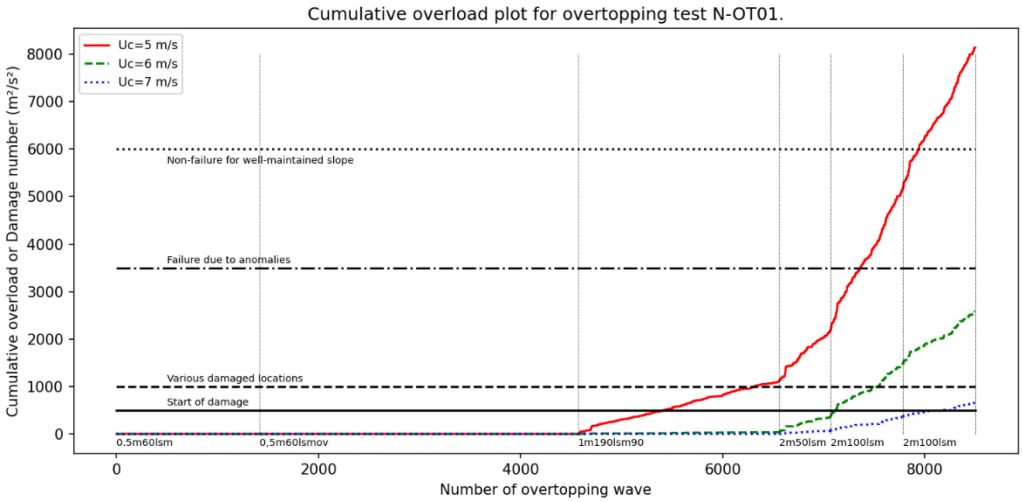

Figure 51 - Cumulative overload function for N-OT01 indicating the damage numbers for three different critical velocities (5, 6 and 7 m/s). The 5 m/s curve (red) is applicable to this site. Each vertical line indicates a transition in wave conditions. The wave condition name (e.g. 0.5m60lsm) is indicated on the graph. The horitontal lines represent the damage qualification as indicated in Table 5.

This project has received funding from the Interreg 2 Seas programme 2014-2020 co-funded by the European Regional Development Fund under subsidy contract No [2S07-023]

5.2.2 N-OT02

The test on N-OT02, containing the wet spot was conducted with wave conditions I, II, III, IV and V (Figure 52). The last wave condition (V, 2m100lsm) was only applied for 1 "storm hour". As earlier described, this eroded faster than what would be predicted by the overload method (for cover layers in good shape), if we consider the soft or wet spot to be an anomaly.

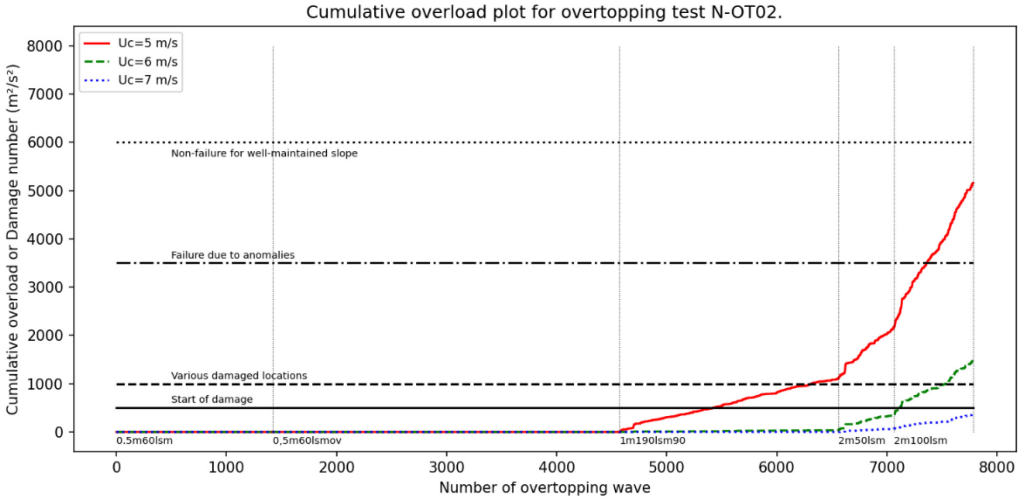

Figure 52 – Cumulative overload function for N-OT02.

5.2.3 N-OT03

Test section N-OT03 contained, in comparison to N-OT01, a large amount of mole burrows. Here, test conditions I, II and III (2x) were applied (Figure 53). During condition II (0.5m60lsmov), erosion of the mole burrows was observed, and barren spots became apparent. The erosion increased during the first application of wave condition III (1m190lsm). In this episode, the gravel drain became visible at the toe. After 3 "storm hours" (i.e., halfway the second run of condition III), no severe damage had developed. Then, an artificial damage was applied: two additional artificial burrows, but even this did not lead to any failure in the subsequent hour of testing. According to the cumulative overload function, serious damage was expected after an overload of 3500 m^2/s^2 but this level of loading was not reached during the test.

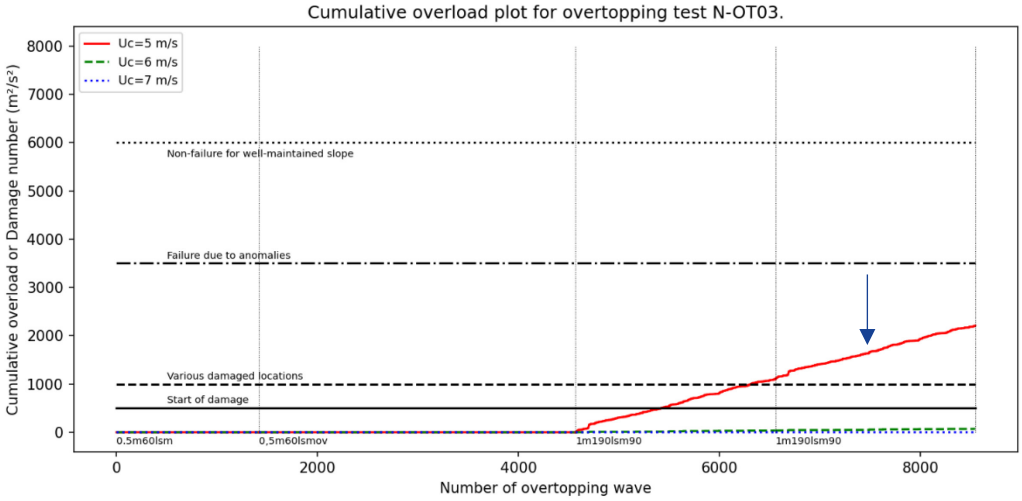

Figure 53 - Cumulative overload function for N-OT03. Arrow indicates introduction of artificial damage.

This project has received funding from the Interreg 2 Seas programme 2014-2020 co-funded by the European Regional Development Fund under subsidy contract No [2S07-023]

5.2.4 N-OT04

On the fourth section, the first part of the test consisted of wave condition I (0.5m60lsm) repeated by wave condition III (1m190lsm) (2x). Some barren patches had appeared during these runs, but no failure had occurred. Failure was not to be expected based on the overload function.

The introduction of a set of artificial burrows (indicated by an arrow on Figure 54) by manual drilling in a wide V-shape so that contact with the sand core was made, quickly led to expulsion of sand at the lower burrows when condition IV (2m50lsm) was applied. This condition was ended after half an hour of simulated storm and was continued with condition III (1m190lsm). Here also, sand expulsion led to undermining of the cover layer and ended with slope failure, but later than predicted by the wave overtopping damage function.

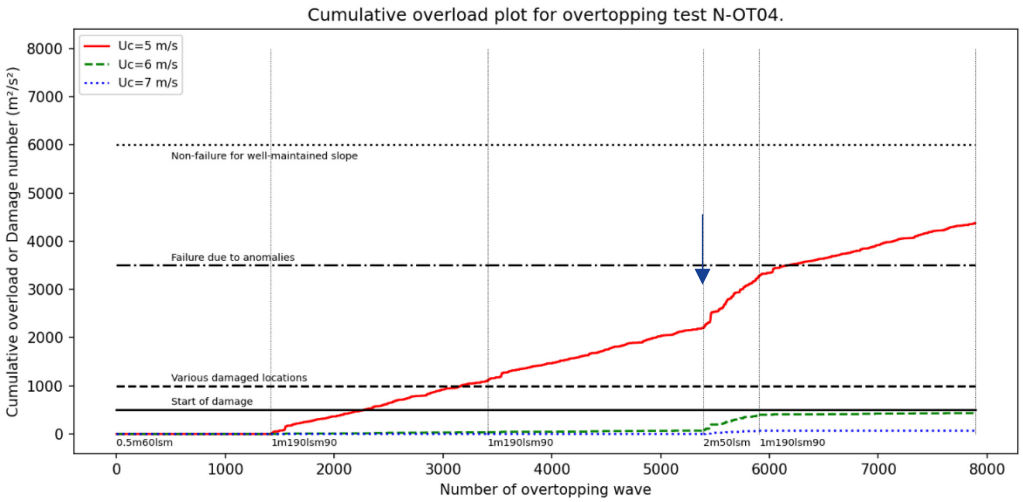

Figure 54 - Cumulative overload function for N-OT04, complete test. Arrow indicates introduction of artificial damage, after which sand explusion starts. The damage function predicts failure shortly after the start of the last storm condition (overtopping wave 6000), but in reality the failure occurred only after the sand expulsion lasted much longer (nearly 2000 additional overtopping waves).

This project has received funding from the Interreg 2 Seas programme 2014-2020 co-funded by the European Regional Development Fund under subsidy contract No [2S07-023]

6 Conclusions

From the preceding chapters, the following insights can be formulated:

1. A well-maintained grass covered levee, in absence of any anomaly (burrow, damage, …) is capable of withstanding 15 to 30 hours of overflow without any significant damage occurring to the vegetation cover; the grass is becoming thinner, and the clay cover becomes increasingly visible, but the integrity of the levee cover is not compromised.
2. Presence of burrows in contact with the sand core are critical: within 1 to 10 hours of overflow, a burrow may lead to critical failure of the levee slope and exposure of the sand core. From the experiments, it is indicated that burrows (mole, rabbit, fox, …) are critical.
3. Presence of a tree standing on the levee toe does not lead to critical damage, notwithstanding the fact that erosion occurs around the tree, exposing shallow tree roots.
4. Presence of soft soil patches (e.g., due to clogged drains, or maybe even small-scale piping), with (or without) longer vegetation (e.g., reed) growing, is a weak spot in the levee slope: the soft soil erodes within minutes, and larger failure may occur within tens of minutes.
5. The length of the vegetation did not significantly impact the outcome of tests, although longer vegetation may obscure unwanted anomalies.
6. During overflow the water accelerate towards the equilibrium velocity. At some test the velocity profile at the surface was measured: for a specific discharge 150 L/s/m to 400 L/s/m the equilibrium velocity measured at the surface increase from approx. 5 m/s tot 6.5 m/s. From the surface velocity a Gauckler-Manning roughness value in between 0.0121 $s/m^{1/3}$ and 0.0128 $s/m^{1/3}$ was derived, considerably lower than the Gauckler-Manning coefficient of 0.020 $s/m^{1/3}$ recommended by the CIRIA manual. A possible explanation could be the difference between the velocity at the surface and the section averaged velocity. It was the goal to gain more insight in the velocity profile within the water column by high-speed recording, but these were unfortunately not successful.
7. A large-scale failure progresses very fast under overflow; within minutes, the collapse depression can travel several meters backwards. During the tests, the overflow was then stopped to prevent the entire levee to become undermined. In real situations, the process would continue; when extrapolating, this leads to the fact that there is no time for emergency actions before the levee section potentially breaches.
8. The overtopping experiments indicate that the tested levees can withstand subsequent storms with one to two hours of wave overtopping of small size waves. Open patches evolve and a gravel drain at the levee toe becomes exposed, but no failure occurs.
9. The presence of anomalies (wet spot, burrows) undermines the strength of the levee slope: erosion occurs faster and may lead to levee slope failure.
10. The thinner clay cover layer of Belgian levees appears to be more prone to undermining and failure than Dutch layers with thicker cover layers.
11. A thick cover layer (in NL: 80 – 100 cm) does not prevent burrowing down to the sand core (but hamper and can reduce the probability of it).
12. The presence of anomalies on the inner (landward) levee slope appears to be an aggravated factor for the levee strength both under overtopping and overflow conditions.

This project has received funding from the Interreg 2 Seas programme 2014-2020 co-funded by the European Regional Development Fund under subsidy contract No [2S07-023]

7 References

Azimi, A.H. & Rajaratnam, N. (2009). Discharge characteristics of weirs of finite crest length. J. Hydraul. Eng., doi: 10.1061/(ASCE)HY.1943-7900.0000117, 1081-1085.

Bazin, H. (1896). Experiences Nouvelles sur l'écoulement par deversoir. Annales des Ponts et Chaussees, 12(2), 645-731.

Chanson, H. (2002). The hydraulics of stepped chutes and spillways. Swets & Zeitlinger: Lisse. ISBN 90-5809-352-2

Chow, V.T. (1959). Open-channel hydraulics. McGraw-Hill Civil Engineering Series. McGraw-Hill: Tokyo

CIRIA. (2013). The International Levee Handbook. Ciria C731. ISBN §. 1332 pp.

Cox, M.B. (1942). Tests on vegetated waterways. Tech. Bull. T-15

Daamen, E.; Heida, L.; Mom, R.; Wauben, C. (2022). Factual report golfoverslag- en grastrekproeven Polder2C's. Versie 3.0. Infram Hydram, Maarn, The Netherlands.

Depreiter, D.; Vercruysse, J.; Verelst, Tsimopoulou, V., K. Koelewijn, A. Zomer W & Peeters, P. (2023a). Polder2C's Overflow tests on Belgian Levees. Factual data report. WL Rapporten WL2023R20_047_2. Waterbouwkundig Laboratorium, Antwerpen, Belgium.

Depreiter, D.; Vercruysse, J.; Verelst, Tsimopoulou, V., K. Koelewijn, A. Zomer W & Peeters, P. (2023b). Polder2C's Overflow tests on Dutch Levees. Factual data report. WL Rapporten WL2023R20_047_3. Waterbouwkundig Laboratorium, Antwerpen, Belgium.

Henderson, F.M. (1966). Open channel flow, Macmillan Series in Ocean Engineering, Prentice Hall: New York, NY. ISBN 978-0-02353-510-9)

Hewlett, H.W..; Boorman, L.A.; Bramley, M.E. (1987). Design of reinforced grass waterways. CIRIA

Hölscher, R & Zomer, W. (2021). Field research on burrows and discontinuities in embankments. BZ Ingenieurs en Managers Report nr. BZ262E.210820.rap.0. (Polder2C's report)

Keller, R.J.; Rastogi, A.K. (1977). Design chart for predicting critical point on spillways. J. Hydraul. Div. ASCE, 103(HY12): 1417–1429

Palmer, V.J. (1945). A method of designing vegetated spillways. Agric. Eng. 26: 516–520

Ree, W.O.; Palmer, V.J. (1949). Flow of water in channels protected by vegetative linings. Technical Bulletin 967

Schall, J.D.; Thompson, P.L.; Zerges, S.M.; Kilgore, R.T.; Morris, J.L. (2012). Hydraulic design of highway culverts. Hydraulic Design Series Number 5. Publication No. FHWA-HIF-12-026 (5): 323. Available at: http://www.fhwa.dot.gov/engineering/hydraulics/pubs/12026/hif12026.pdf

Tracy, H.J. (1957). Discharge Characteristics of Broad-Crested Weirs: Washington, D.C. 21 pp.

Tsimopoulou, V. & Koelewijn, A (2022). Management of harmful animal activities on levees: Fact finding fieldwork in the Living Lab Hedwige-Prosperpolder. (Polder2C's report)

Van Cauter, P.-J. (2021). Field tests of flow overtopping a dike: flow characteristics on landward slope. Universiteit Gent.

Van der Meer, J.W.; B. Hardeman; Steendam, G.J.; Schtrumpf, H. & Verheij, H. (2010). Flow depths and velocities at crest and inner slope of a dike, in theory and with the Wave Overtopping Simuator. ASCE, Proc. ICCE 2020, Shangai.

Vercruysse, J.; Depreiter, D.; Lopez Castaño, S.; Peeters, P. (2023). Design and application of a steady overflow generator (Polder2C's). WL Rapporten WL2022R20_047_1. Waterbouwkundig Laboratorium, Antwerpen, Belgium.

This project has received funding from the Interreg 2 Seas programme 2014-2020 co-funded by the European Regional Development Fund under subsidy contract No [2S07-023]